2006

Performance of torus-type brushless DC motor with winding connected in two and three-phase system

Dinakar Choppa
Louisiana State University and Agricultural and Mechanical College

PERFORMANCE OF TORUS-TYPE BRUSHLESS DC MOTOR WITH WINDING CONNECTED IN TWO AND THREE-PHASE SYSTEM

A Thesis
Submitted to the Graduate Faculty of the
Louisiana State University and
Agricultural and Mechanical College
in partial fulfillment of the
requirements for the degree of
Master of Science in Electrical Engineering

in

The Department of Electrical & Computer Engineering

by
Dinakar Choppa
Bachelor of Engineering, Andhra University, April 2003
August, 2006

Acknowledgements

First of all I would like to express my heartfelt and deepest appreciation to my advisor and major professor Dr. Ernest A. Mendrela for his invaluable suggestions and constant guidance. I also thank Dr. Hsiao-Chun Wu and Dr. Ashok Srivastava for sparing their time to be a part of my defense committee.

I would also thank Dr. Hallie Dozier and Dr. Chunyan Li, for supporting me through out my stay here at LSU.

I would like to express my gratitude towards my family members for their support and I also thank my friends who made my stay at LSU a pleasant one.

Table of Contents

Acknowledgements……..ii

List of Tables……...v

List of Figures……vi

Abstract…….. x

Chapter 1 : Introduction 1
1.1 Brushless DC Motors 1
1.2 Contributions of the Thesis 4
1.3 Outline of the Thesis 5

Chapter 2 : Torus Type Brushless DC Motors 7
2.1 Literature Review 7
2.2 Torus Type Motor: Construction and Principle of Operation 9
2.3 Design Data of the Motor Under Study 13
2.3.1 Motor With Three-Phase Winding Connection 15
2.3.2 Motor With Two-Phase Winding Connection 20

Chapter 3 : Performance of Torus Motor with the Winding Connected In Three - Phase System 24
3.1 Analysis in Dynamic Conditions 24
3.1.1 Dynamic Model of the Motor 24
3.1.2 Parameters of Electrical Circuit and Mechanical System 31
3.1.3 Simulation of Motor Dynamics 32
3.2 Performance of the Motor in Steady-State Condition 37
3.2.1 Motor Model for Steady-State Operation 37
3.2.2 Performance Characteristics of the Motor 38
3.3 Influence of Switching Angle of Inverter Transistors on Motor Performance……..42

Chapter 4 : Performance of Torus Motor with the Winding Connected In Two - Phase System 47
4.1 Analysis in Dynamic Conditions 47
4.1.1 Dynamic Model of the Motor 47
4.1.2 Parameters of Electrical Circuit and Mechanical System 52
4.1.3 Simulation of Motor Dynamics 54
4.2 Influence of Switching Angle of Inverter Transistors on Motor Performance……..61

Chapter 5 : Conclusions 66

References. 69

Appendix A: Matlab Programs for Three Phase Motor 71

Appendix B: Matlab Programs for Two Phase Motor 75

Appendix C: SIMULINK Block Diagrams for Three Phase 79

Appendix D: SIMULINK Block Diagrams for Two Phase 80

Vita……..... 81

List of Tables

Table 2.1 Main design data of the motor under study 16

Table 3.1 Parameters of the electrical and mechanical system..... 32

Table 3.2 Electromechanical parameters at rated supply and rated load..... 42

Table 4.1 Parameters of the electrical and mechanical system..... 53

Table 4.2 Electromechanical parameters at rated supply and rated load..... 62

List of Figures

Fig. 1.1 Brush and Brushless DC Motors 2

Fig. 1.2 Disassembled view of a brushless DC motor [5] 6

Fig. 1.3 Basic topologies of AFPM machines: (a) single-sided slotted machine, (b) double-sided slotless machines with internal stator and twin PM motor, (c) double- sided slotted stator and internal PM rotor, (d) double- sided coreless motor with internal stator. 1-stator core, 2-stator winding, 3-rotor, 4-PM, 5-frame, 6-bearing, 7-shaft [4]. 6

Fig. 2.1 Single sided disc type machines: 1-laminated stator, 2-PM, 3- rotor, 4- frame, 5-shaft, 6- sheave; (a) single-sided motor (b) single-sided motor integrated with sheave and brake [4] 8

Fig. 2.2 (a) Double-sided AFPM brushless machine with internal disc rotor: 1-rotor, 2-PM, 3- stator core, 4- stator winding (b) rotor and stator configuration [4] 9

Fig. 2.3 Layout of torus motor [8] 10

Fig. 2.4 Scheme of the torus- type permanent magnet motor: 1-stator core, 2- stator winding, 3-rotor, 4- magnets (a) cross- sectional view (b) PM distribution (c) multi- stack motor [10] 10

Fig. 2.5 Distribution of coils and hall sensors on the torus core 11

Fig. 2.6 Distribution of permanent magnet on the rotor disc 12

Fig. 2.7 Simplified machine model [11] 12

Fig. 2.8 (a) 2D [6] and (b) 3D flux directions of the non-slotted torus machine 13

Fig. 2.9 Scheme of the motor 14

Fig. 2.10 Stator core with Gramme's winding 14

Fig. 2.11 Part of the stator core with teeth [12] 16

Fig. 2.12 PM distribution with respect to a three-phase winding 17

Fig. 2.13 Scheme of stator winding connection in three-phase system 17

Fig. 2.14 Converter circuit for three-phase winding (electronic commutator) 18

Fig. 2.15 EMFs induced and current waveforms for a three-phase winding 19

Fig. 2.16 Magnetomotive force distribution for $t = t_2$ and $t = t_4$ 19

Fig. 2.17 Scheme of rotor magnet distribution in two-phase winding motor 20

Fig. 2.18 Scheme of stator winding connection in two-phase winding motor 21

Fig. 2.19 Converter circuit for two-phase winding (electronic commutator) 21

Fig. 2.20 Waveforms of electromotive forces induced and current waveforms for a two-phase winding 22

Fig. 2.21 Magnetomotive force distribution for two-phase winding at two time instants t_1 and t_2 and the relevant paths of the currents in phases A and B 23

Fig. 3.1 Circuit diagram of supply-inverter-motor system 25

Fig. 3.2 Scheme to equation 3.6 26

Fig. 3.3 Position of the rotor with respect to the phase A 28

Fig. 3.4 SIMULINK model of brushless DC motor 33

Fig. 3.5 SIMULINK Model of the inverter-motor circuit subsystem 34

Fig. 3.6 Waveforms of rotary speed and source current 34

Fig. 3.7 Waveforms of rotary speed and phase current 35

Fig. 3.8 Waveforms of EMF (e_a) and the armature voltage (V_a) 35

Fig. 3.9 Waveforms of armature current (i_a) and armature voltage (V_a) 36

Fig. 3.10 Waveforms of total torque (T_{em}) and phase torque (T_a) 36

Fig. 3.11 Waveforms of EMFs in the 3phases and the armature voltage (V_a) 37

Fig. 3.12 Equivalent circuit of the motor in the steady state conditions 38

Fig. 3.13 Electromagnetic characteristics determined from the dynamic simulation in steady-state 40

Fig. 3.14 Electromechanical characteristics obtained from steady state model 41

Fig. 3.15 Illustration of the switching angle β (a) zero switching angle (b) switching angle β 43

Fig. 3.16 Supply current (i_s) vs load torque (T_L) 44

Fig. 3.17 Output power (P_m) vs load torque (T_L) 44

Fig. 3.18 Efficiency (*Eff)* vs load torque (T_L) 45

Fig. 3.19 Electromechanical characteristics of the motor for β = -10° 46

Fig. 4.1 Circuit diagram of supply-inverter-motor system 47

Fig. 4.2 Scheme to equation 4.1 48

Fig. 4.3 Position of the rotor with respect to the phase 'A' 49

Fig. 4.4 SIMULINK model of two-phase brushless DC motor 54

Fig. 4.5 SIMULINK model of the inverter-motor circuit subsystem 55

Fig. 4.6 Waveform of rotary speed and source current 56

Fig. 4.7 Waveform of rotary speed and phase current 56

Fig. 4.8 Waveform of EMF (e_a) and the armature voltage (V_{sa}) 57

Fig. 4.9 Waveforms of armature current (i_a) and supply voltage (v_{sa}) 57

Fig. 4.10 Waveforms of total torque (T_{em}) and phase torque (T_a) 58

Fig. 4.11 Waveforms of EMFs in the two phases and the supply voltage (v_{sa}) 58

Fig. 4.12 Electromagnetic characteristics determined from the dynamic simulation in steady-state 59

Fig. 4.13 Electromechanical characteristics obtained from steady-state model 61

Fig. 4.14 Illustration of the switching angle β (a) zero switching angle (b) switching angle β 63

Fig. 4.15 Supply current (i_s) vs load torque (T_L) 63

Fig. 4.16 Output power (P_m) vs load torque (T_L) 64

Fig. 4.17 Efficiency (*Eff*) vs load torque (T_L) 65

Fig. 4.18 Electromechanical characteristics of the motor for β = -10° 65

Abstract

A torus-type permanent magnet brushless DC motor is the object of this thesis. The motor can operate with the winding connected either in two – phase or three – phase system. A comparative study of performance of the motor operating in these two systems is the objective of the thesis.

To analyze the motor performance, the dynamic models of the motors operating with two – phase and three – phase motors have been proposed. The simulation of motor operation was carried out using the MATLAB/SIMULINK software package.

A study of motors operation in steady state conditions has been done by applying simpler models which were based on brush DC motor equivalent circuit. It is observed that the electromechanical characteristics of these two motors are similar and the motor with three – phase winding has lesser quantity of torque ripples.

Since the motors operating in the two types winding connection systems are supplied from voltage – type inverters, switching conditions have a significant influence on motor performance. This was also studied in the thesis project using the dynamic motor model. The results of this study show that by advancing the commutation angle, the efficiencies could be improved greatly.

Chapter 1 : Introduction

1.1 Brushless DC Motors

Nowadays, Brushless Direct Current (BLDC) are becoming prominent as the demand for efficiency, precise speed and torque control, reliability and ruggedness increases. BLDC provide high efficiency and exemplary precision of control when compared to conventional motors. It has the best torque vs. weight or efficiency characteristics. They are used in military, grinding, aircraft, automotive applications, communications equipment etc [1]. The theory of brushless dc motors was proposed in 1962 by T.G. Wilson and P. H. Trickey. But the limitations in magnet and power switching have prevented them to bring into real life. In 1980, Powertec Industrial Corporation started manufacturing them [2] [3].

Brushless, as the name implies there are no brushes and commutators (see Fig. 1.1). In conventional motors, the switching of current in the armature coils is done using the combination of brushes and commutators whereas in the brushless, the commutation is performed with the help of electronic circuit, which reduces the mechanic losses and improves the efficiency. There are many other merits of brushless motors over the conventional motors.

- The brushless machines requires hardly any maintenance

- Speed/torque characteristics are flat which enables operation at all speeds with rated load. Whereas brushed dc motors have moderately flat characteristics.
- The electric noise generation is low for brushless.
- Brushless motors have low rotor inertia which improves dynamic response.
- They have higher speed range and output power to frame size ratio.

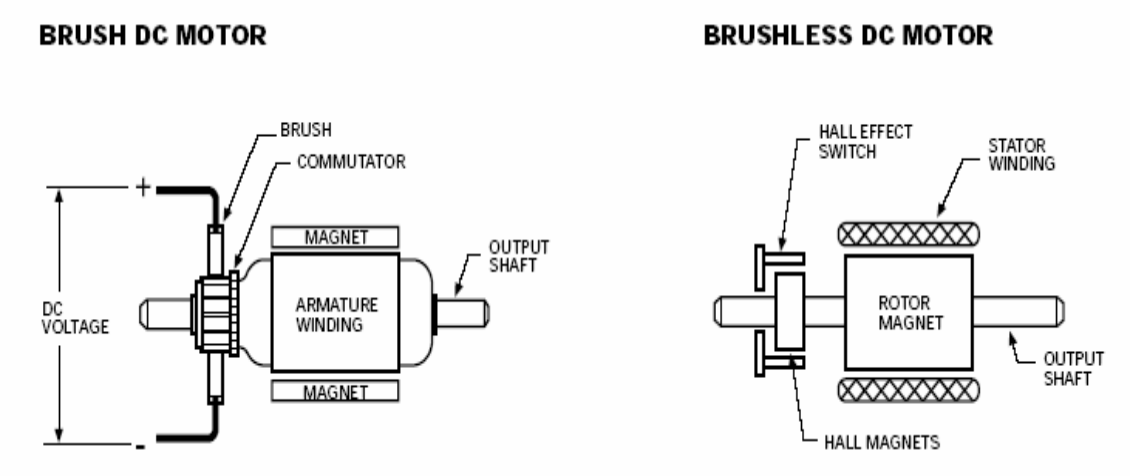

Fig. 1.1 Brush and Brushless DC Motors

The brushless disc type dc motors are classified into:

- Radial flux permanent magnet machines (RFPM).
- Axial flux permanent magnet machines (AFPM).

An example of radial flux BLDC motor is shown in Fig. 1.2. An important part of the motor is position sensor which controls the switching of the power electronic switches. In Fig. 1.2, hall elements are used for this purpose.

The BLDC axial flux machines may be classified [4] as follows:

- Single-sided AFPM machines
    - with slotted stator (Fig. 1.3a)
    - with slotless stator
    - with salient-pole stator
- Double-sided AFPM machines
    - with internal stator (Fig. 1.3b)
        - with slotted stator
        - with slotless stator
            - with iron core stator
            - with coreless stator (Fig. 1.3d)
            - without both rotor and stator cores
        - with salient pole stator
    - with internal rotor (Fig. 1.3c)
        - with slotted stator
        - with slotless stator
        - with salient pole stator
- multi-stage (multidisc) AFPM machines

This project deals with a torus type brushless dc motor, shown schematically in Fig. 1.3b. Torus is a double-sided, axial-flux, disc type permanent-magnet, brushless machine which may be operated as either a motor or a generator. It has a simple toroidal, stripwound stator core which carries a slotless, polyphase winding. Use of the high-field

permanent - magnet material Neodymium-Iron-Boron for excitation enables quite high flux density to be achieved in the relatively large air gap associated with the slotless winding [7].

The winding coils are spread uniformly on the stator core and can be connected in single or poly-phase systems. In this project, motors with two-phase and three-phase connection of the winding are analyzed.

1.2 Contributions of the Thesis

The objectives of this project are:

- To compare the performance of torus-type DC motor with winding connected in two and three-phase system.
- To analyze the motor operation under variable load conditions.

The tasks accomplished in this project are:

- Literature study about the torus brushless dc motor.
- Determination of motor parameters of the equivalent circuit and mechanical system for two and three phase winding.
- Formulation of the mathematical motor models for steady and dynamic operation.
- Development of block diagrams for simulation of 2-phase and 3-phase motor dynamics using MATLAB/SIMULINK.
- Simulation of motor operation under variable load.

- Determination of the average values of electromechanical quantities and presenting them in the form of the following characteristics: current, speed, input power, output power, efficiency vs. load torque.
- Comparison of motor characteristics operating with a winding connected in two and three phase system.

1.3 Outline of the Thesis

- Chapter 2 gives a description about the torus type brushless dc motors. Design data of the motor under study. Winding connection of the two and three phase systems.
- Chapter 3 focuses on the performance of 3-phase motor which is determined from the simulation based on dynamic and steady-state models of the motor. Influence of switching angle of inverter transistors on motor performance is also studied.
- Chapter 4 presents the performance of torus motor with the winding connected in two phase system. Influence of switching angle on motor performance is also analyzed.
- Chapter 5 contains the comparative study of performance of the motor operating in two and three phase winding connection and summarizes the conclusions.

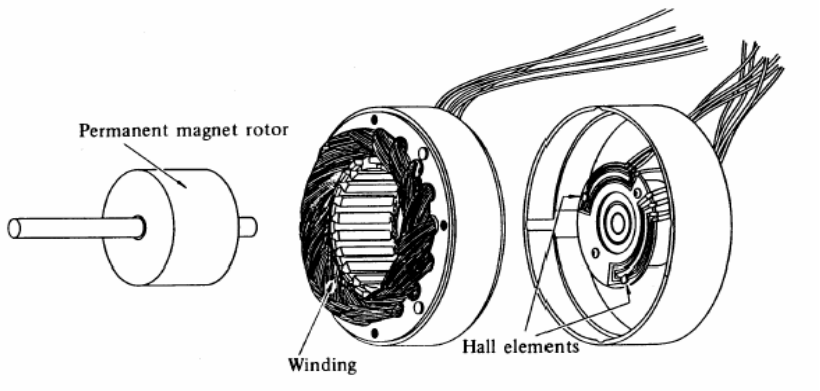

Fig. 1.2 Disassembled view of a brushless DC motor [5]

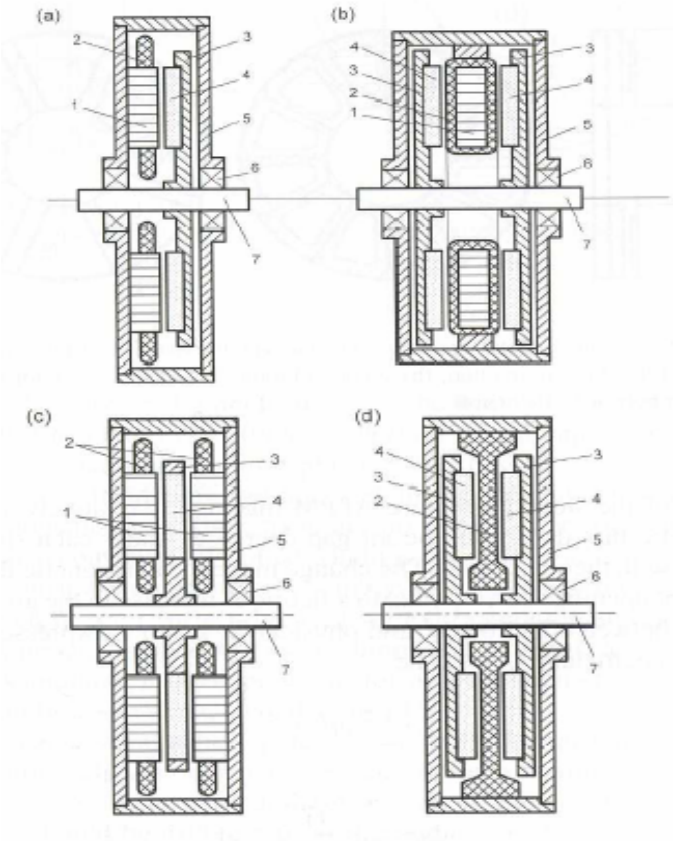

Fig. 1.3 Basic topologies of AFPM machines: (a) single-sided slotted machine, (b) double-sided slotless machines with internal stator and twin PM motor, (c) double-sided slotted stator and internal PM rotor, (d) double- sided coreless motor with internal stator. 1-stator core, 2-stator winding, 3-rotor, 4-PM, 5-frame, 6-bearing, 7-shaft [4].

Chapter 2 : Torus Type Brushless DC Motors

2.1 Literature Review

Due to compact structure, pancake shape and high power density, the AFPM is used as an alternative to the cylindrical RFPM. The AFPM is also called as disc-type machine [4]. The AFPM have various advantages over the RFPM. They have high power-to-weight ratio with less core material [6], planar and variable air gaps. By varying the direction of the main air gap flux many discrete topologies can be derived. They produce less noise and vibration levels than that of conventional machines. They are used in naval and domestic applications like pumps, fans, valve control, electrical vehicles, centrifuges, machine tools. These machines can be used in low speed applications such as electromechanical traction drives, hoists or wind generators because a number of poles can be accommodated. There are many topologies of the machine and the machine topology is determined by magnetic or non-magnetic stator. The machines may single-sided, double-sided machines with internal PM disc rotor, double-sided machines with internal ring-shaped core stator, with slotted or coreless stator. The single-sided construction of an axial flux machine is simple than the double-sided one, but the torque production capacity is lower. Fig. 2.1 shows typical constructions of single-sided AFPM brushless machines with surface PM rotors and laminated stators wound from electromechanical steel strips.

In the double-sided machine with internal PM disc rotor, the armature winding is located on two stator cores as shown in Fig. 2.2. The disc with PMs rotates between two

stators [4]. PMs are embedded or glued in a nonmagnetic rotor skeleton and the nonmagnetic air gap is large. The stators can be connected in parallel or series connection. Parallel connected stators can operate even if one stator winding is broken. But a series connection is preferred because it can provide equal but opposing axial attractive forces.

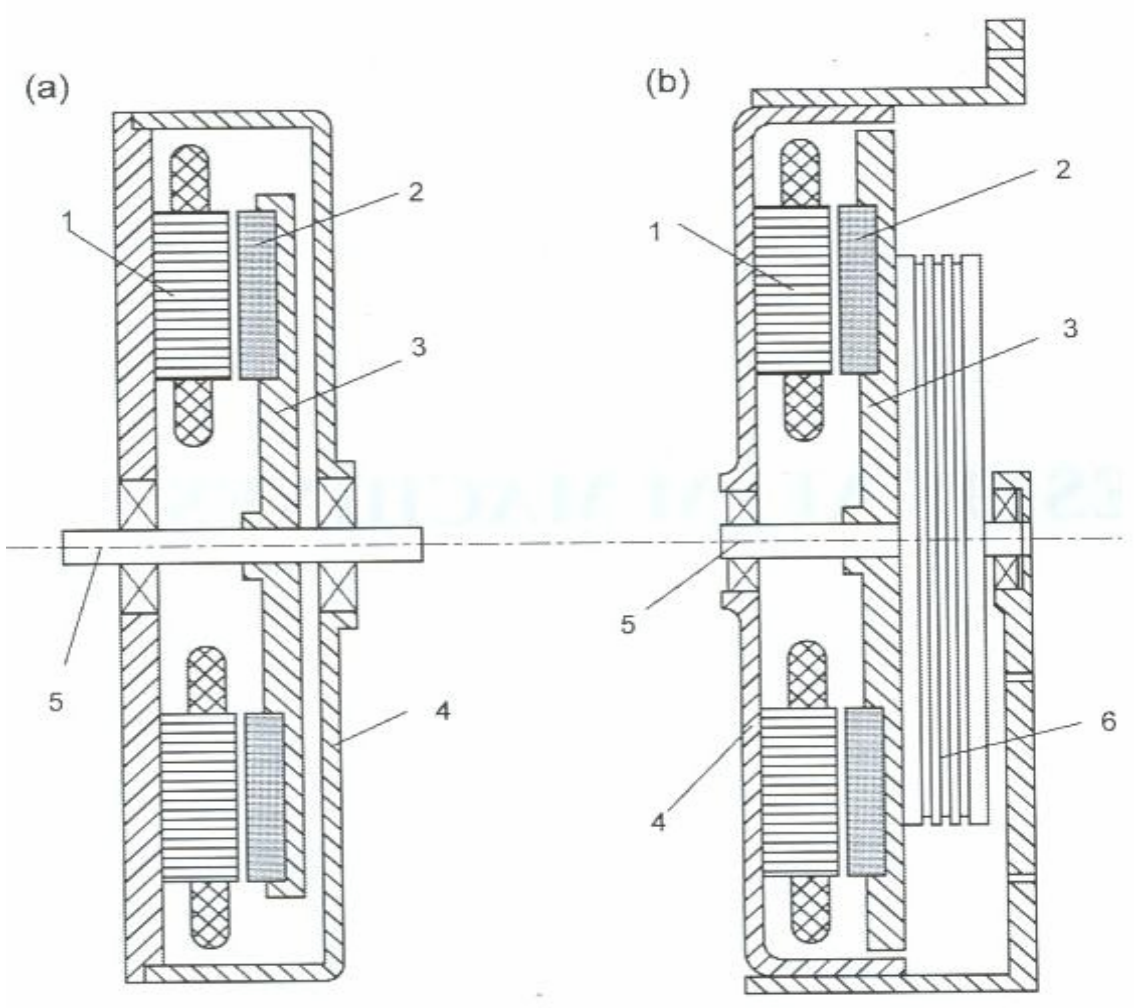

Fig. 2.1 Single sided disc type machines: 1-laminated stator, 2-PM, 3- rotor, 4-frame, 5-shaft, 6- sheave; (a) single-sided motor (b) single-sided motor integrated with sheave and brake [4]

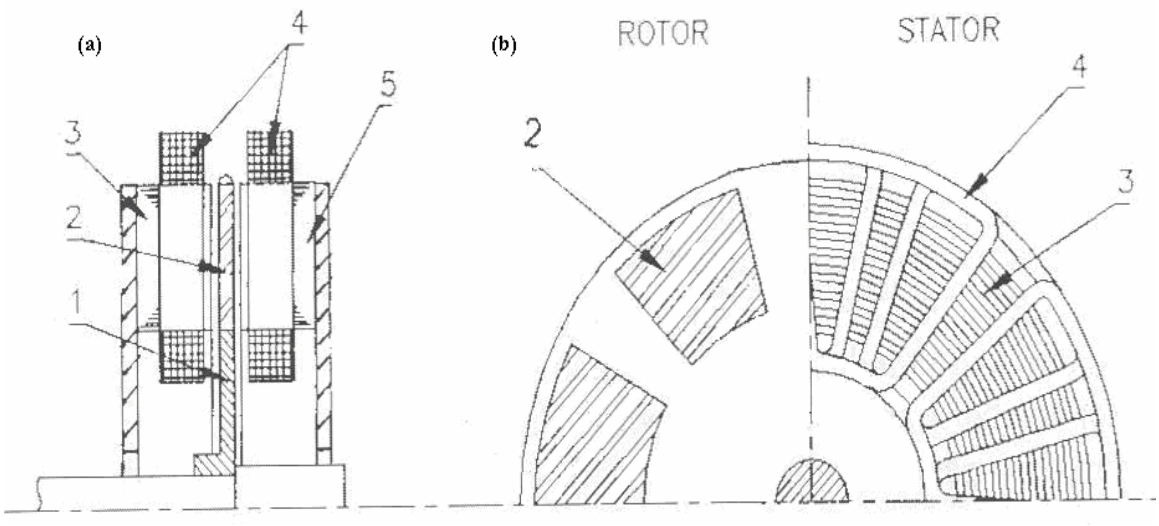

Fig. 2.2 (a) Double-sided AFPM brushless machine with internal disc rotor: 1-rotor, 2-PM, 3- stator core, 4- stator winding (b) rotor and stator configuration [4]

2.2 Torus Type Motor: Construction and Principle of Operation

The motor under consideration in this thesis is a torus motor. Torus is a lightweight compact electrical machine which acts as a brushless dc motor when it is supplied with a suitable power electronic switching circuits. It is a double-sided, axial-flux, disc-type, permanent-magnet machine with toroidal, strip-wound stator core which carries a slotless, polyphase winding [13]. Due to the absence of stator slots, the cogging torque, pulsation losses in the rotor, acoustic noise components and flux ripple are absent [7]. The slotless winding provides low phase self and mutual inductances because of large magnetic gap [8]. The stator resistances are low because of short end-winding length. Fig. 2.3 and Fig. 2.4 show the basic layout of a torus motor.

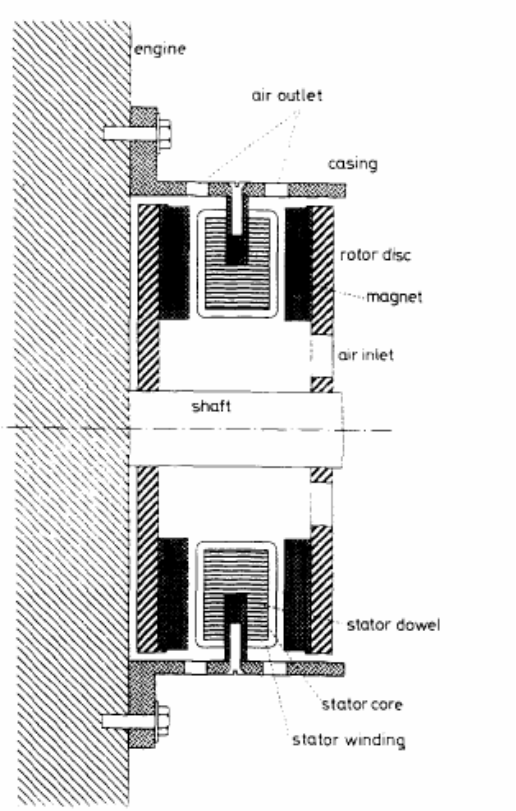

Fig. 2.3 Layout of torus motor [8]

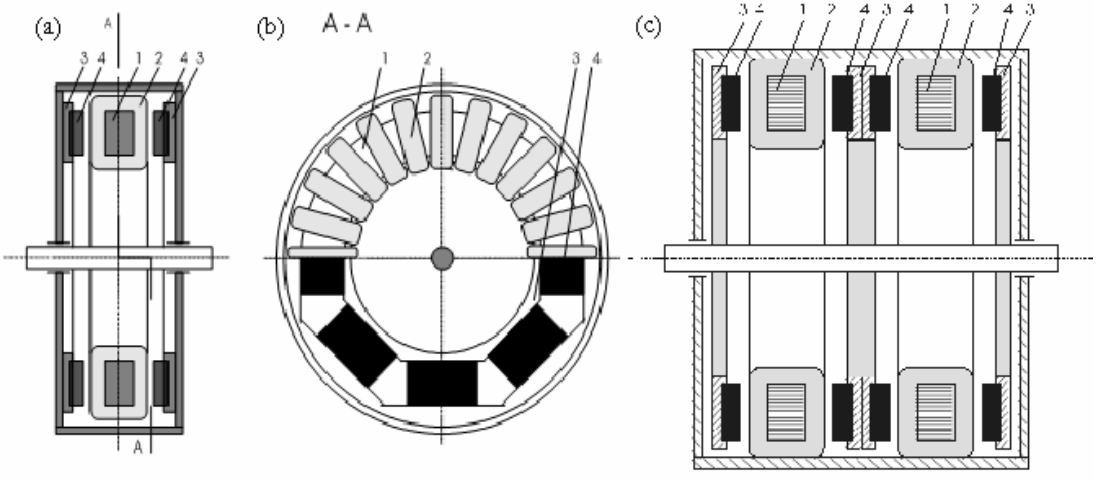

Fig. 2.4 Scheme of the torus- type permanent magnet motor: 1-stator core, 2- stator winding, 3-rotor, 4- magnets (a) cross- sectional view (b) PM distribution (c) multi-stack motor [10]

The stator core is wound with a number of coils as shown in Fig. 2.5 below. The stator coils can be connected either in single-phase or in polyphase winding. To detect the rotor position, optical sensors or hall position sensors are used. They are displaced by 120° (electrical) as shown in Fig. 2.5 or by 60° (electrical). The hall sensors detect the rotor position and trigger the corresponding transistors to switch on corresponding stator winding. For a machine with two rotor discs, permanent magnets are arranged circumferentially around each rotor disc with N-S-N-S arrangement. The schematic diagram in Fig. 2.6 shows the distribution of the magnets on the rotor discs. If the curvature of the machine is ignored, a simplified model of the machine can be visualized as shown in the Fig. 2.7, where the x-coordinate represents the circumferential direction and the y-coordinate represents axial direction [11].

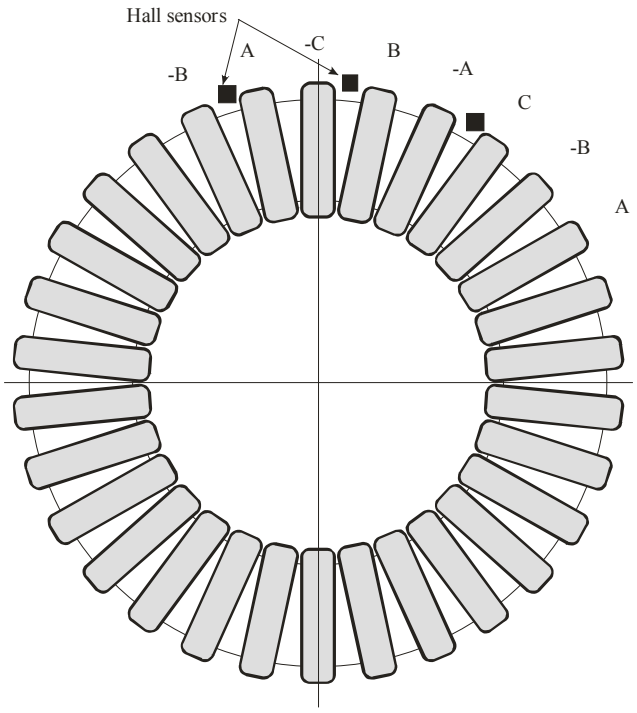

Fig. 2.5 Distribution of coils and hall sensors on the torus core

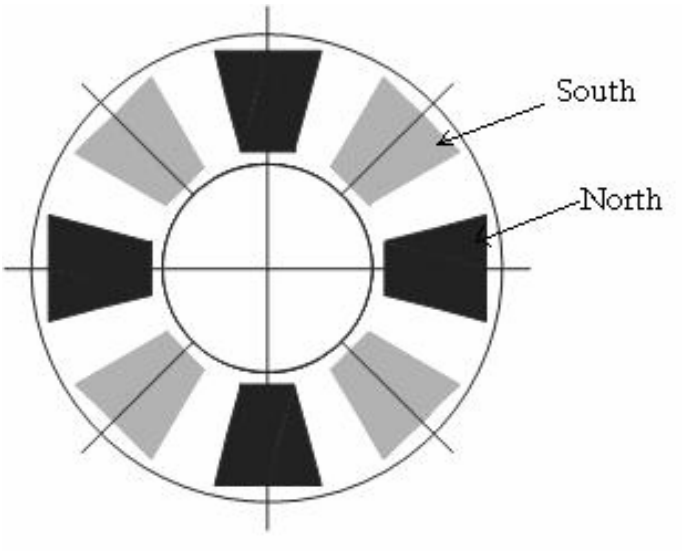

Fig. 2.6 Distribution of permanent magnet on the rotor disc

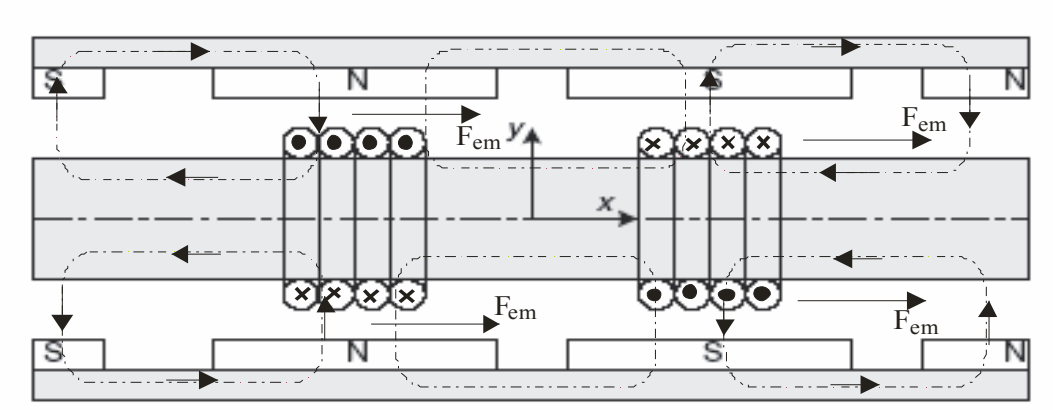

Fig. 2.7 Simplified machine model [11]

The north magnet on one disc is placed directly opposite to a north magnet on the other disc. When the N magnet produces the flux, it is directed axially across the two air gaps into the stator core. Then the flux travels circumferentially along the strip-wound core (stator core) and enters the opposite pole (S pole) of the permanent magnets of the rotor core [6] [11]. An interaction of magnetic flux and currents flowing in the coils, which

contributes to the electromagnetic force F_{em} that acts in one direction, is shown in Fig. 2.7. The 2D and 3D flux directions of the non-slotted torus machine are shown in Fig. 2.8.

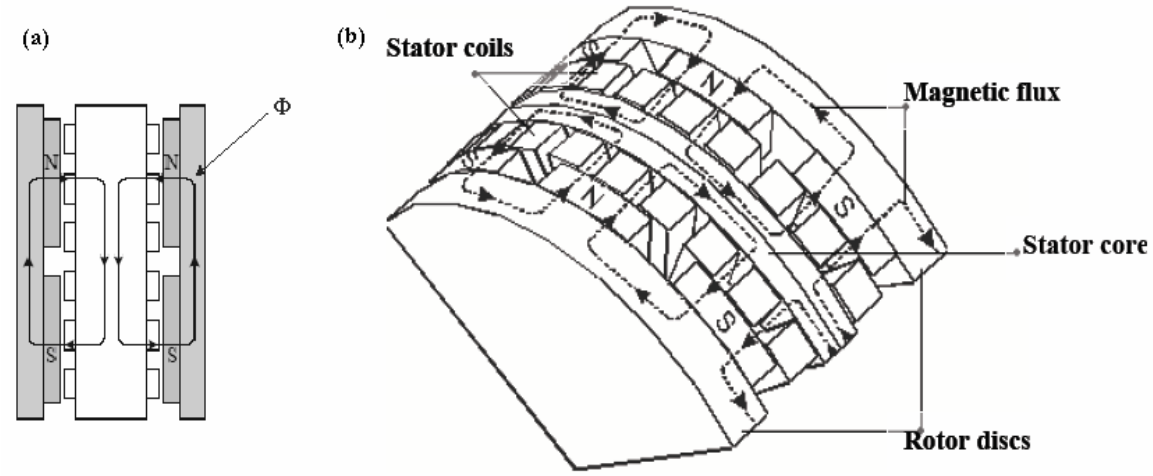

Fig. 2.8 (a) 2D [6] and (b) 3D flux directions of the non-slotted torus machine

2.3 Design Data of the Motor Under Study

The motor considered in this project comprises of a stator placed in between two rotor discs. The scheme of the motor with the main design data is shown in Fig. 2.9. The construction of the motor is described in the previous section where schematic diagrams are presented. A series of permanent magnets are placed circumferentially on the rotor disc. The stator coils are connected either in three-phase winding or two-phase winding with hall sensors placed at 120° and 90° (electrical angle) respectively. The power supply wires, which are connected to the stator winding are lead through the hollow shaft. The scheme of the stator is shown in Fig. 2.10.

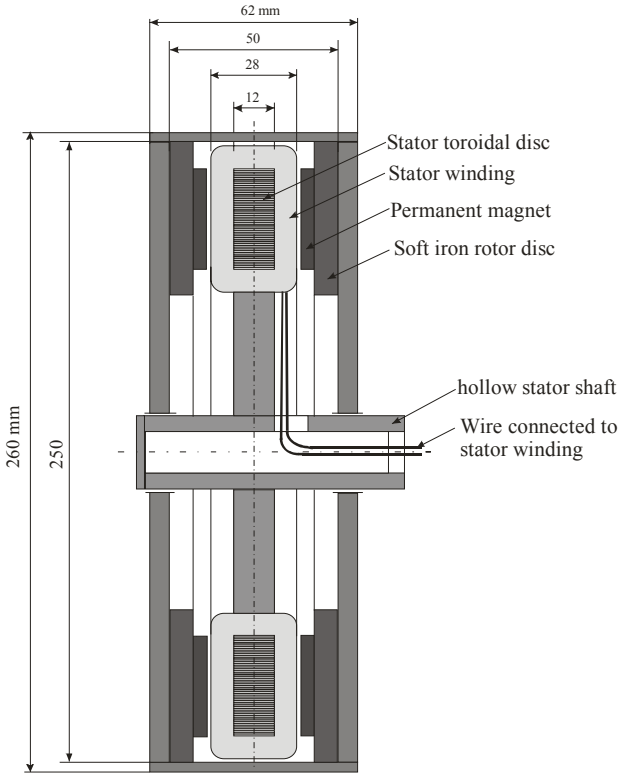

Fig. 2.9 Scheme of the motor

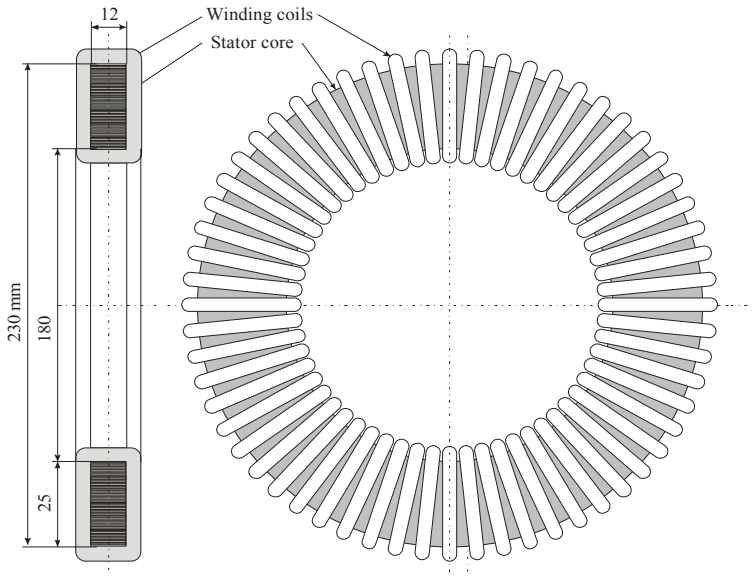

Fig. 2.10 Stator core with Gramme's winding

The torus motors have typically slotless winding which ensures zero cogging torque. To strengthen the magnetic field and to increase the torque, the ferromagnetic teeth are added between the coils. This however contributes to the increase of torque ripple. This can be reduced by applying square shaped magnets instead of trapezoidal shape. A part of the stator core with teeth is shown in Fig. 2.11. The main design data of the motor under study is shown Table 2.1.

2.3.1 Motor with Three-Phase Winding Connection

As mentioned in the previous sections, the motor comprises a slotless toroidal core wound with three-phase winding. The rotor is of disc shape and embraces the stator. The permanent magnets are placed on the rotor circumferentially. Fig. 2.12 shows the basic scheme of the rotor permanent magnet distribution with respect to the in three-phase winding system. Fig. 2.13 shows the scheme of the winding connection of stator. The hall sensors are distributed along the stator at 120° (electrical) to sense the position of the rotor [14]. This is shown in Fig. 2.13. The three-phase motor is driven through a DC/AC converter (inverter) which uses six transistors arranged in a three-phase bridge configuration as shown in Fig. 2.14. Each transistor conducts for 120° electrical which implies each armature phase conducts with either positive or negative polarity for 120° electrical in a sequential manner to cause the motor to rotate [15]. The transistors switching On/Off time is neglected and assumed to be zero.

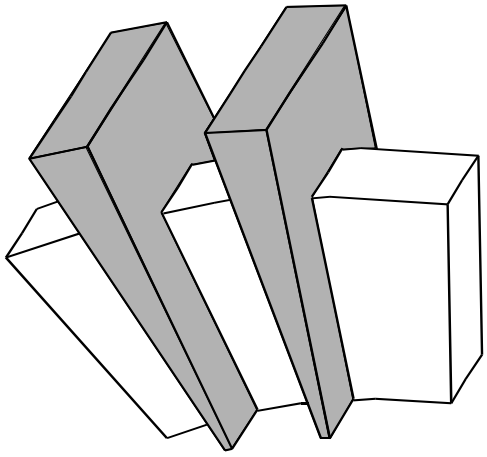

Fig. 2.11 Part of the stator core with teeth [12]

Table 2.1 Main design data of the motor under study

Stator:	
Laminated core:	
Outer diameter of the stator core	D_o=230mm
Inner diameter of the stator core	D_{in}=180mm
Thickness	t_s = 12mm
Number of coils	N_c=60
Number of turns in the coil	N_t=13
Air-gap length	g=1mm
Rotor:	
Soft iron discs:	
Outer diameter	d_o = 250mm
Inner diameter	d_{in} = 160mm
Thickness	t_r = 7mm
Permanent magnets of rectangular shape:	
Length	l = 25mm
Width	b = 20mm
Thickness	t_m = 4mm
B_r = 1.18 T, H_c = 900 KA/m	

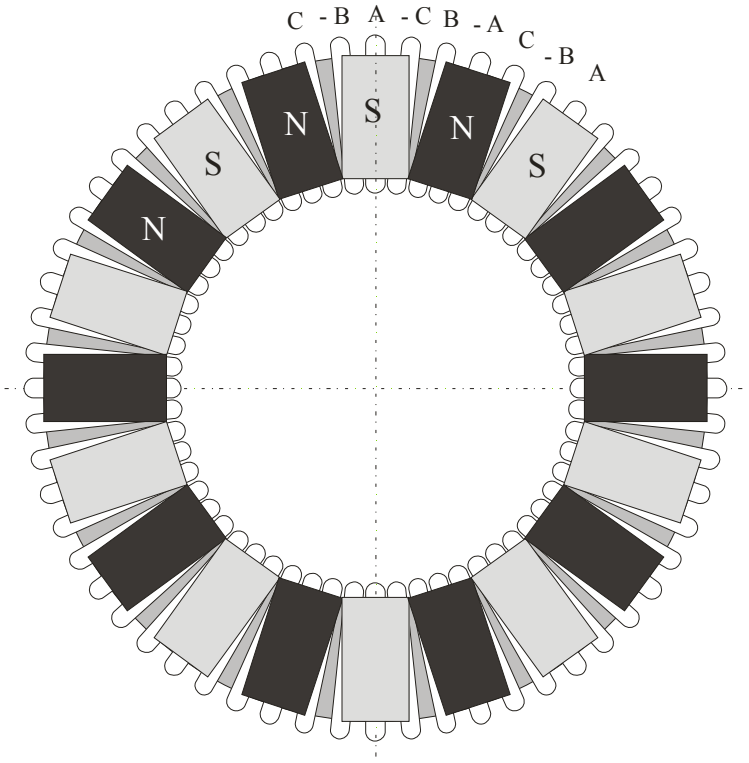

Fig. 2.12 PM distribution with respect to a three-phase winding

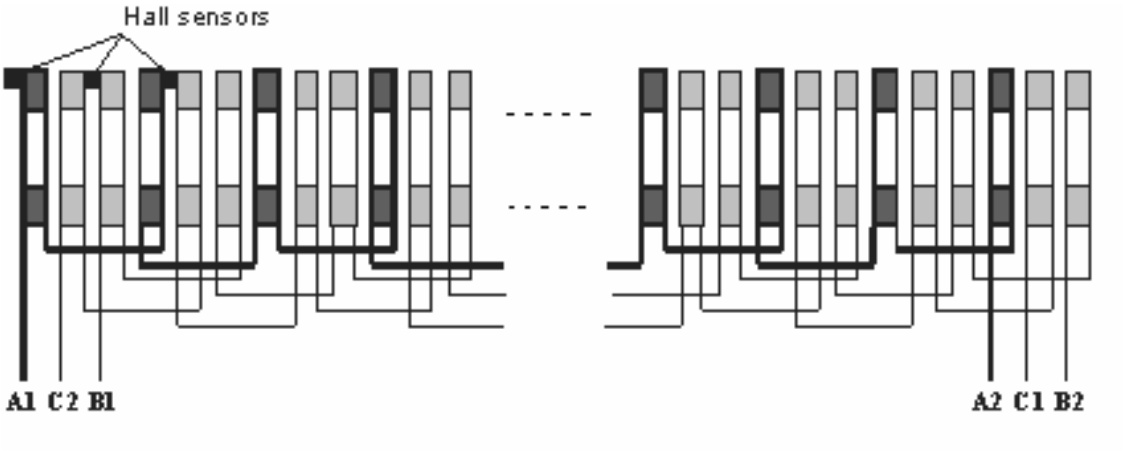

Fig. 2.13 Scheme of stator winding connection in three-phase system

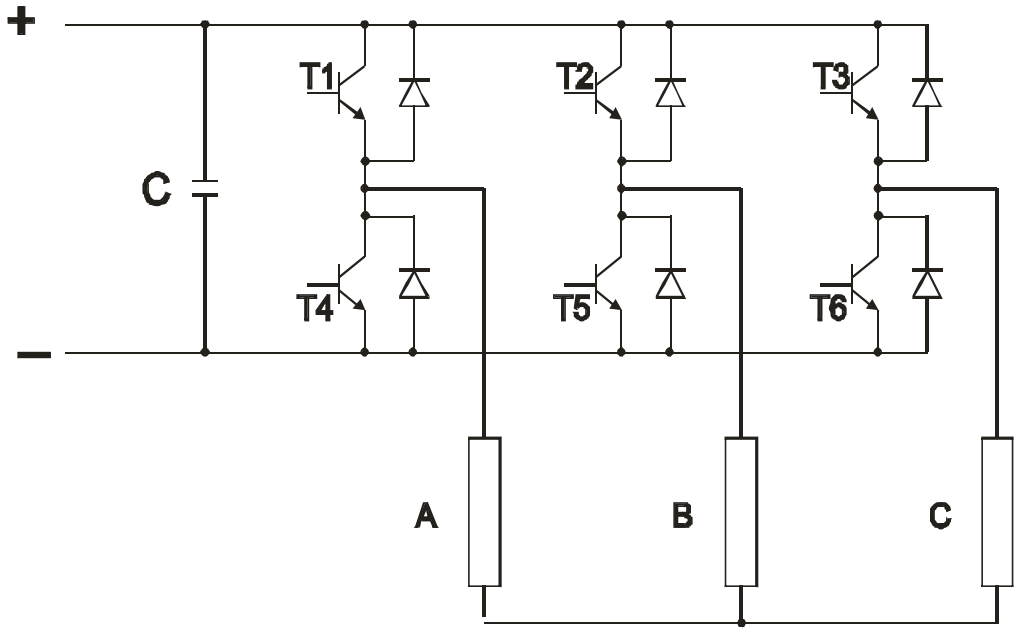

Fig. 2.14 Converter circuit for three-phase winding (electronic commutator)

Since the transistors switching time (On/Off) is assumed to be zero at any time, there are always two phases connected across the d.c. terminals through two transistors leaving the third phase disconnected. Fig. 2.15 shows the back EMF induced in the winding and current waveforms for a three-phase winding. For a three-phase system, each phase current is displaced in time at an angle of 120° electrical from one another. Fig. 2.16 shows the distribution of the resultant magnetomotive force F along the angle θ for the time instant $t = t_2(\theta = 60°)$ (see Fig. 2.15) when the phases A & B are switched by the transistors 1 & 5. The third phase C is disconnected from the circuit. At time $t = t_4(\theta = 120°)$, transistors 1 & 6 are switched and the phases A & C are connected and the phase B is disconnected.

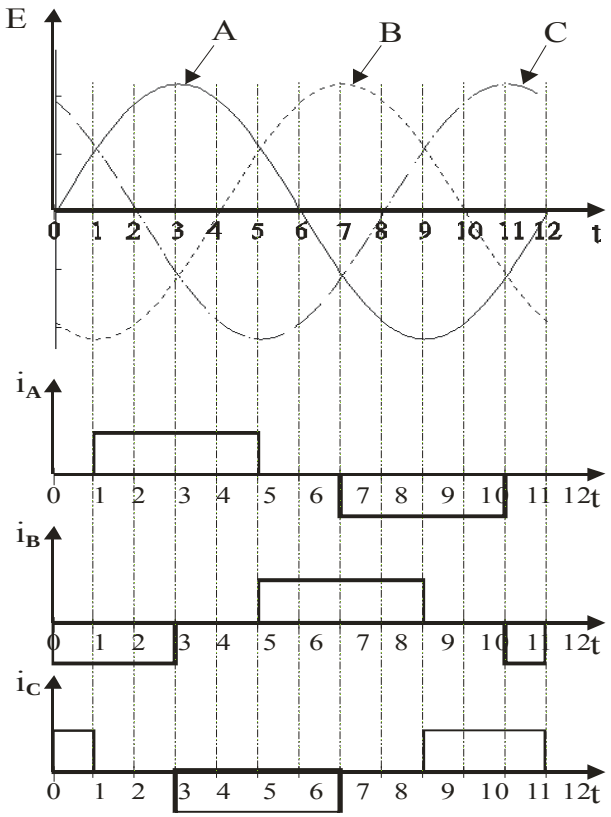

Fig. 2.15 EMFs induced and current waveforms for a three-phase winding

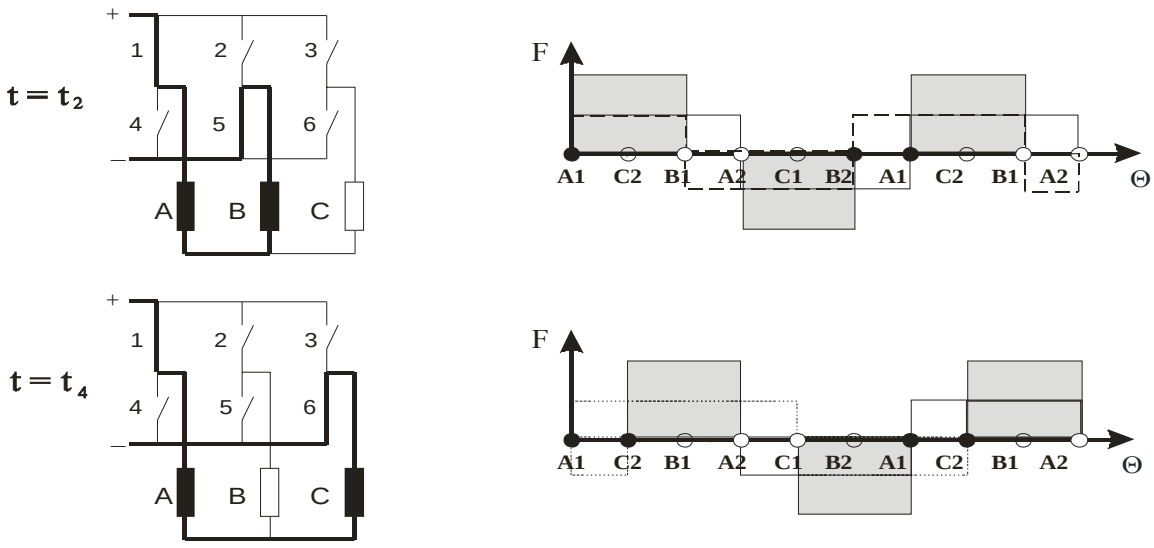

Fig. 2.16 Magnetomotive force distribution for $t = t_2$ and $t = t_4$

2.3.2 Motor With Two-Phase Winding Connection

The rotor magnet distribution for a two-phase winding system considered in this section is shown in Fig. 2.17 and two-phase stator winding connection is shown in Fig. 2.18. The two-phase system is also supplied with an electronic commutator (inverter), which uses 8 transistors arranged in H-shaped configuration in two stages, shown in Fig. 2.19. Each stage operates for 90° electrical angle, which implies that each armature phase conducts for 90° electrical angle either with positive or negative polarity.

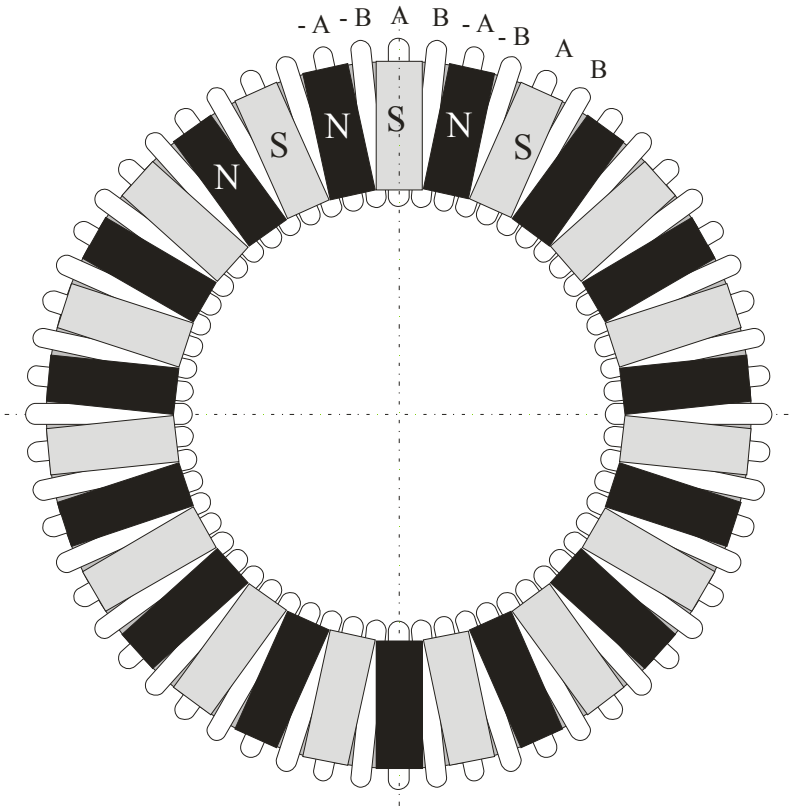

Fig. 2.17 Scheme of rotor magnet distribution in two-phase winding motor

The back EMFs induced in the two phases are displaced by 90° in time. The currents should be supplied accordingly. In general, the duty cycle for each current can be

different. Fig. 2.20 shows when each phase conducts current over the 90°. Thus, only one phase is connected to the supply at any instant of time.

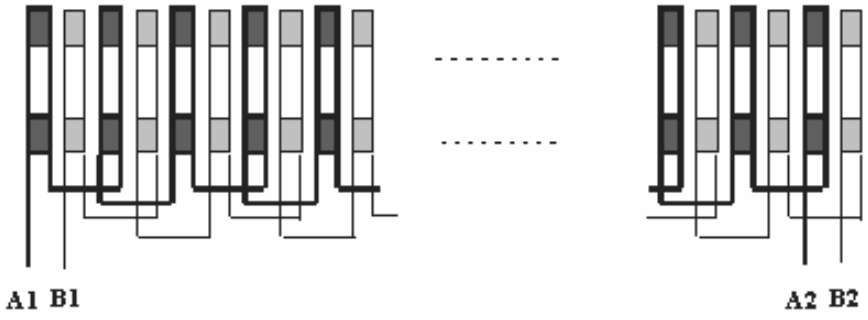

Fig. 2.18 Scheme of stator winding connection in two-phase winding motor

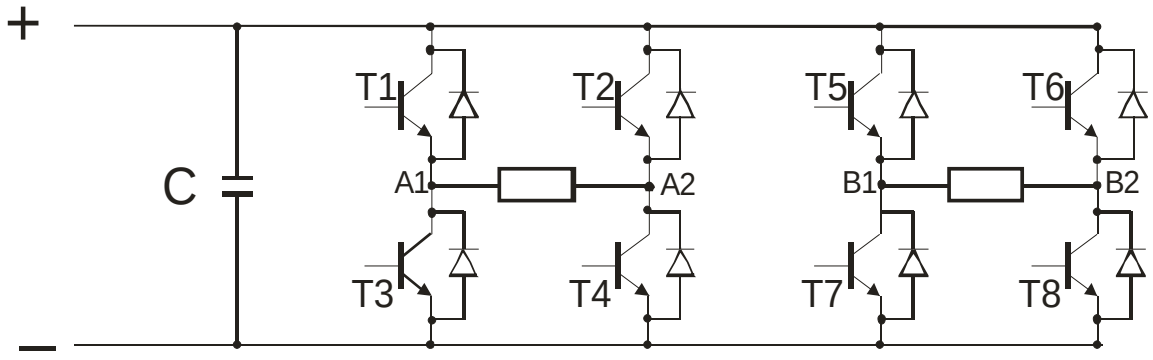

Fig. 2.19 Converter circuit for two-phase winding (electronic commutator)

For phase A, at time $t = t_1$ transistors 1 & 4 are switched on and the phase A winding conducts in positive direction. When it conducts in the negative direction, transistors 2 & 3 are switched on. Similarly, for phase B, at time $t = t_2$ transistors 5 & 8 are switched on and the phase B winding conducts in positive direction and for the negative current transistors 6 and 7 are conducted. Fig. 2.21 shows the diagram of switched transistors for particular time instants t_1 and t_2 and the relevant distribution of magnetomotive forces produced by switched phases.

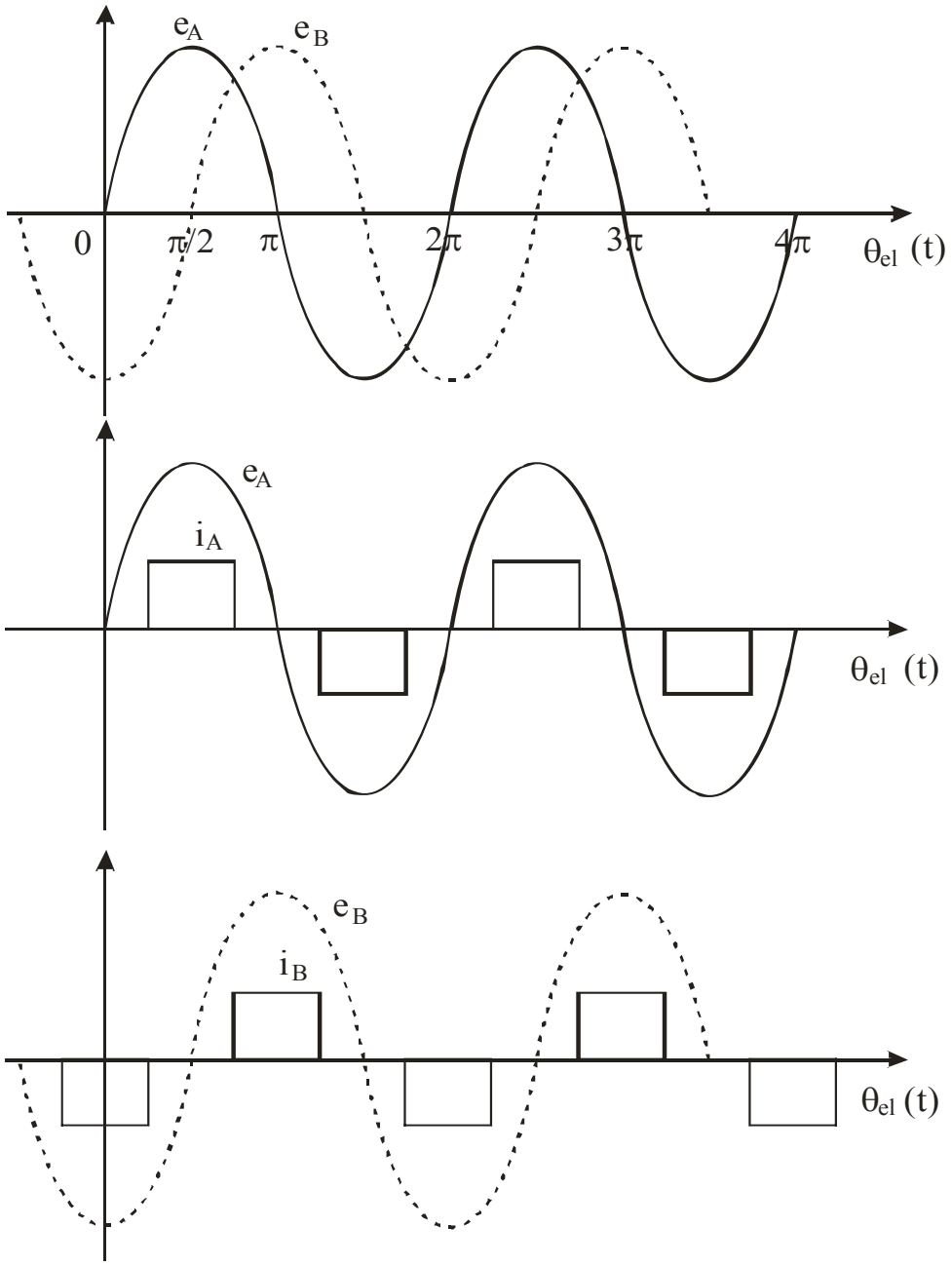

Fig. 2.20 Waveforms of electromotive forces induced and current waveforms for a two-phase winding

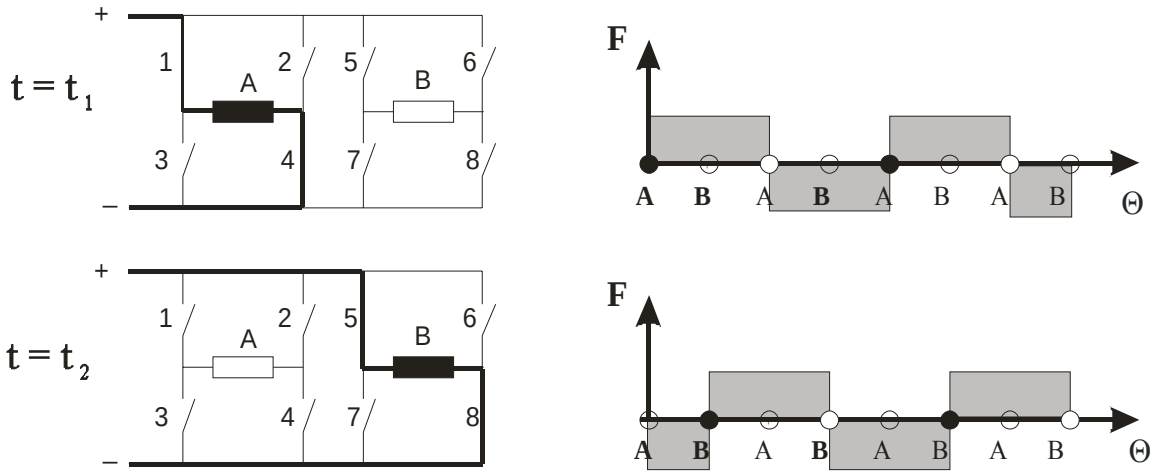

Fig. 2.21 Magnetomotive force distribution for two-phase winding at two time instants t_1 and t_2 and the relevant paths of the currents in phases A and B

Chapter 3 : Performance of Torus Motor with the Winding Connected In Three - Phase System

3.1 Analysis in Dynamic Conditions

3.1.1 Dynamic Model of the Motor

The BLDC motor is supplied from battery through the inverter. The dynamic model of this system is shown in Fig. 3.1. It is derived under the following assumptions:

- All the elements of the motor are linear and core losses are neglected [13] [16].
- Induced currents in the rotor due to stator harmonic fields are neglected [9].
- The electromotive force e_a varies sinusoidally with the rotational electric angle θ_e.
- The cogging torque of the motor is negligible.
- Due to the surface mounted permanent magnets, winding inductance is constant (doesn't change with the electric angle θ_e).
- Voltage drop across the diodes, transistors and the connecting wires are ignored.

All above mentioned assumptions are practically satisfied. The magnetic and electric circuit is linear within the range of operation. Power losses in the inverter are practically negligible since the switching frequency of this low speed motor is low. Also the cogging torque doesn't exist since there is coreless winding.

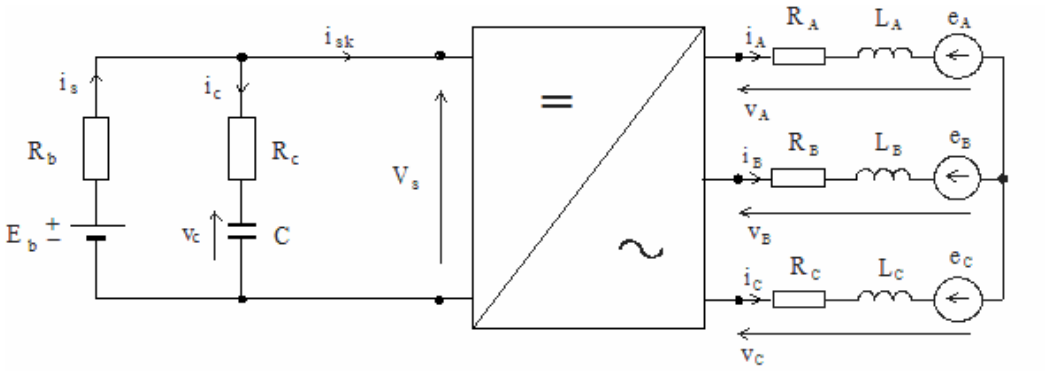

Fig. 3.1 Circuit diagram of supply-inverter-motor system

The equations that describe the model are as follows:

Voltage equations:

- voltage equation at the source side:

$$E_b - i_s \cdot R_b - i_c \cdot R_c = 0 \tag{3.1}$$

$$v_s = v_c + i_c \cdot R_c \tag{3.2}$$

$$i_s = i_{sk} + i_c \tag{3.3}$$

where:

E_b and R_b – voltage and resistance of the source (battery)

R_c – resistance in the capacitor circuit

i_s – source circuit current

i_{sk} – converter input current

v_c – voltage across capacitor

$$v_c = \frac{Q_c}{C} \tag{3.4}$$

Q_c – charge in capacitor,

C – capacitance,

i_c – current flowing through the capacitor:

$$i_c = \frac{dQ_c}{dt} \tag{3.5}$$

- Voltage equations at the motor side (Fig. 3.2) are:

$$\begin{aligned} v_A &= v_N + v_{sA} \\ v_B &= v_N + v_{sB} \\ v_C &= v_N + v_{sC} \end{aligned} \tag{3.6}$$

where:

v_{sA}, v_{sB}, v_{sC} are the inverter output voltages that supply the 3 – phase winding.

v_A, v_B, v_C are the voltages across the motor armature winding.

v_N – voltage at the neutral point.

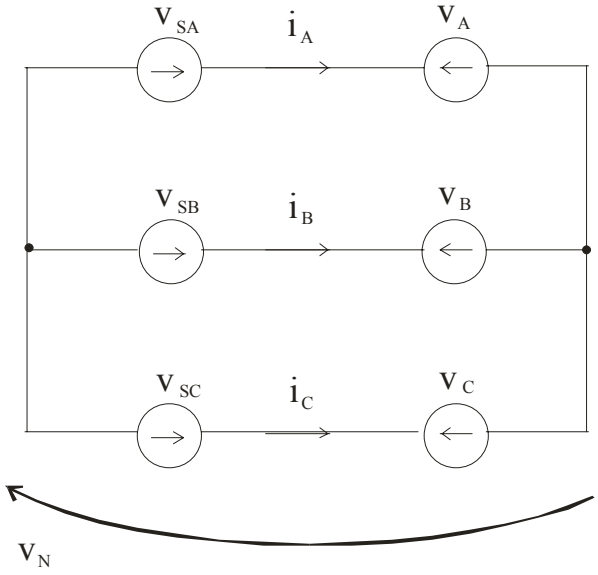

Fig. 3.2 Scheme to equation 3.6

The equation of the voltages across the motor winding

$$\begin{bmatrix} v_A \\ v_B \\ v_C \end{bmatrix} = \begin{bmatrix} R_A & 0 & 0 \\ 0 & R_B & 0 \\ 0 & 0 & R_C \end{bmatrix} \begin{bmatrix} i_A \\ i_B \\ i_C \end{bmatrix} + \frac{d}{dt} \begin{bmatrix} L_A & L_{AB} & L_{AC} \\ L_{BA} & L_B & L_{BC} \\ L_{CA} & L_{CB} & L_C \end{bmatrix} \begin{bmatrix} i_A \\ i_B \\ i_C \end{bmatrix} + \begin{bmatrix} e_A \\ e_B \\ e_C \end{bmatrix} \tag{3.7}$$

or in shorter version:

$$\mathbf{V_a} = \mathbf{R_a} \cdot \mathbf{I_a} + \frac{\mathbf{d}}{\mathbf{dt}} \mathbf{L_a} \cdot \mathbf{I_a} + \mathbf{E_a} \tag{3.8}$$

Since the resistances R_a of all phases are the same:

$$\mathbf{R_a} = \begin{bmatrix} R_a & 0 & 0 \\ 0 & R_a & 0 \\ 0 & 0 & R_a \end{bmatrix} \tag{3.9}$$

Since the self- and mutual inductances are constant for surface mounted permanent magnets and the winding is symmetrical:

$$L_A = L_B = L_C = L; \textit{ and } L_{AB} = L_{BC} = L_{CA} = L_{BA} = L_{AC} = L_{CB} = M$$

the inductance matrix takes the form:

$$\mathbf{L_a} = \begin{bmatrix} L & M & M \\ M & L & M \\ M & M & L \end{bmatrix} \tag{3.10}$$

For Y connected stator winding:

$$i_a + i_b + i_c = 0$$

Thus the voltage equation takes the form:

$$\begin{bmatrix} v_A \\ v_B \\ v_C \end{bmatrix} = \begin{bmatrix} R_A & 0 & 0 \\ 0 & R_B & 0 \\ 0 & 0 & R_C \end{bmatrix} \begin{bmatrix} i_A \\ i_B \\ i_C \end{bmatrix} + \frac{d}{dt} \begin{bmatrix} L_s & 0 & 0 \\ 0 & L_s & 0 \\ 0 & 0 & L_s \end{bmatrix} \begin{bmatrix} i_A \\ i_B \\ i_C \end{bmatrix} + \begin{bmatrix} e_A \\ e_B \\ e_C \end{bmatrix} \tag{3.11}$$

where $L_s = L - M$ synchronous inductance.

Since $L = L_l + L_m$ and $M = -(1/2)\, L_m$, the synchronous inductance

$$L_s = L_l + (3/2)\, L_m \tag{3.12}$$

where:

L_l – leakage inductance

L_m – magnetizing inductance

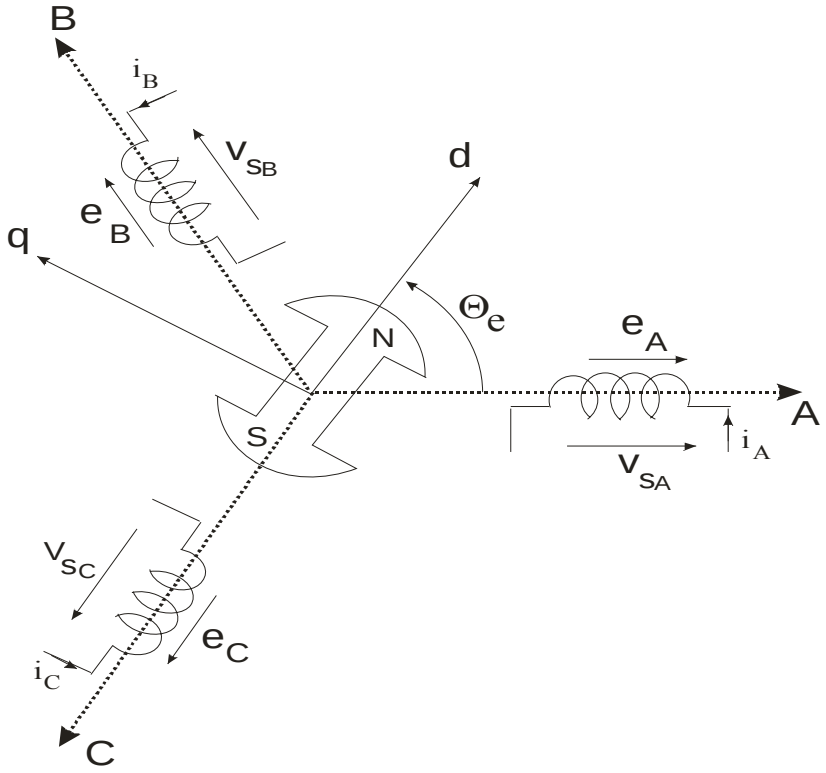

Fig. 3.3 Position of the rotor with respect to the phase A

The electromotive force induced in the phase *A* winding (see Fig. 3.3):

$$e_a = K_E \omega_m \sin(\theta_e) \tag{3.13}$$

where:

K_E – constant,

ω_m – rotor angular speed:

$$\omega_m = \frac{1}{p}\frac{d\theta_e}{dt} \tag{3.14}$$

θ_e – electrical angle (Fig.3.3),

p – number of pole pairs.

For three-phase winding the electromotive forces written in a form of matrix $\boldsymbol{E_a}$

$$E_a = \frac{K_E}{p}\begin{bmatrix} \sin\theta_e \\ \sin(\theta_e - \frac{2}{3}\pi) \\ \sin(\theta_e - \frac{4}{3}\pi) \end{bmatrix}\frac{d\theta_e}{dt} \tag{3.15}$$

Equation that links the supply and motor sides:

$$i_{sk} = \frac{1}{v_s}(i_A v_{sA} + i_B v_{sB} + i_C v_{sC}) \tag{3.16}$$

which is derived from the equality of the powers at input and output of the inverter.

Supply voltages for the phases (v_{sA}, v_{sB} and v_{sC}) results from the operation of converter.

Motion equation:

$$T_J + T_D + T_S + T_L = T_{em} \tag{3.17}$$

where:

- Inertia torque:

$$T_J = J\frac{d\omega_m}{dt} \tag{3.18}$$

J – moment of inertia,

- Viscous friction torque

$$T_D = D \cdot \omega_m \tag{3.19}$$

D – friction coefficient,

- Coulomb friction torque

$$T_s = sign(\omega_m) T_d \tag{3.20}$$

T_L - load torque

- Electromagnetic torque for 3-phase motor

$$T_{em} = \frac{e_A i_A}{\omega_m} + \frac{e_B i_B}{\omega_m} + \frac{e_C i_C}{\omega_m} \tag{3.21}$$

$$T_{em} = \frac{e_A i_A}{\omega_m} + \frac{e_B i_B}{\omega_m} + \frac{e_C i_C}{\omega_m} = K_E (f_a(\phi_e).i_A + f_b(\phi_e).i_B + f_c(\phi_e).i_C) \tag{3.22}$$

where

$$f_a(\phi_e) = \sin(\theta_e)$$
$$f_b(\phi_e) = \sin(\theta_e - \frac{2 \cdot \pi}{3})$$
$$f_c(\phi_e) = \sin(\theta_e - \frac{4 \cdot \pi}{3})$$

Combining all the above equations, the system in state-space form [9] is

$$\dot{x} = Ax + Bu \tag{3.23}$$

$$x = \begin{bmatrix} i_A & i_B & i_C & \omega_m & \theta_e \end{bmatrix}^t \tag{3.24}$$

$$A=\begin{bmatrix} -\frac{R_s}{L_s} & 0 & 0 & -\frac{K_E(f_a(\phi_e))}{L_s} & 0 \\ 0 & -\frac{R_s}{L_s} & 0 & -\frac{K_E(f_b(\phi_e))}{L_s} & 0 \\ 0 & 0 & -\frac{R_s}{L_s} & -\frac{K_E(f_c(\phi_e))}{L_s} & 0 \\ \frac{K_E(f_a(\phi_e))}{J} & \frac{K_E(f_b(\phi_e))}{J} & \frac{K_E(f_c(\phi_e))}{J} & -\frac{D}{J} & 0 \\ 0 & 0 & 0 & \frac{P}{2} & 0 \end{bmatrix} \tag{3.25}$$

$$B=\begin{bmatrix} \frac{1}{L_s} & 0 & 0 & 0 \\ 0 & \frac{1}{L_s} & 0 & 0 \\ 0 & 0 & \frac{1}{L_s} & 0 \\ 0 & 0 & 0 & -\frac{1}{J} \\ 0 & 0 & 0 & 0 \end{bmatrix} \tag{3.26}$$

$$L_s = L - M \tag{3.27}$$

$$u = \begin{bmatrix} v_A & v_B & v_C & T_L \end{bmatrix}^t \tag{3.28}$$

3.1.2 Parameters of Electrical Circuit and Mechanical System

The power to the inverter-motor system is supplied from a 24V battery with a capacitor connected in parallel as shown in Fig. 3.1. The parameters of electrical and mechanical system are given below in Table 3.1.

Table 3.1 Parameters of the electrical and mechanical system

Parameters of the supply system:	
EMF of the battery	$E_b = 24\ V$
Source resistance	$R_s = 0.0005\ \Omega$
Resistance in series with capacitor	$R_c = 10\ \Omega$
Capacitance	$C = 0.00001\ F$
Parameters of the motor circuit:	
Phase resistance of the brushless DC motor	$R_a = 0.25\ \Omega$
Leakage inductance	$L_l = 0.1mH$
Magnetizing inductance	$L_m = 1.1mH$
Synchronous inductance	$L_s = L_l + 3/2(L_m) = 0.00175\ H$
EMF constant	$K_e = E_m / \omega_m = 0.628\ V/ (rad/s)$
Parameters of the mechanical system:	
Moment of inertia	$J = 0.021\ Kg/m^2$
Friction coefficient	$D = 0.004\ N{\cdot}m/ (rad/s)$
Rated torque	$T_{load} = 10\ N{\cdot}m$

3.1.3 Simulation of Motor Dynamics

The block diagram of the motor is built using MATLAB/SIMULINK in accordance with the mathematical model derived in section 3.1. The block diagram of the model is shown in Fig. 3.4.

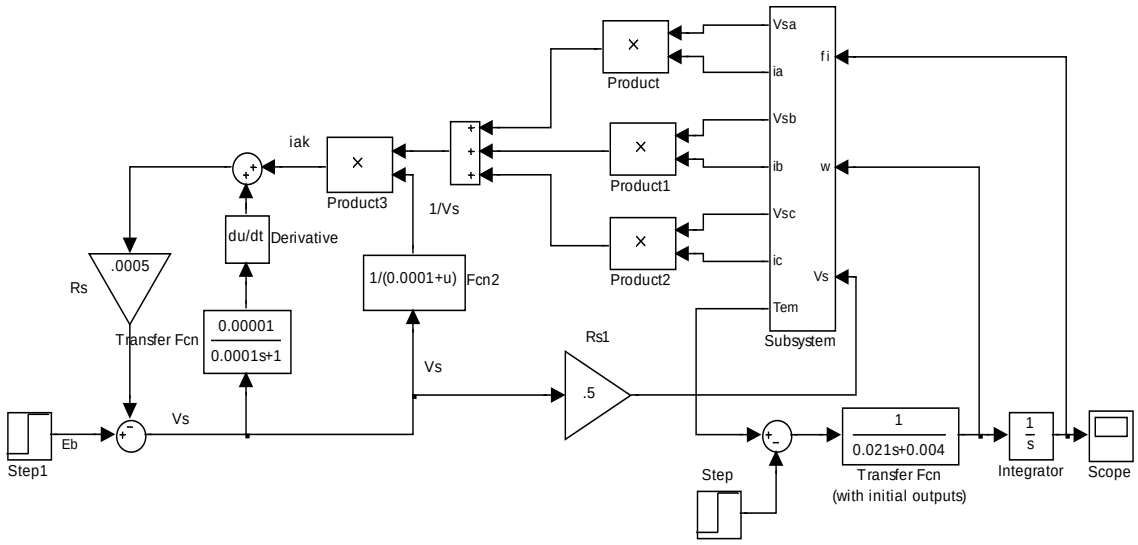

Fig. 3.4 SIMULINK model of brushless DC motor

The main block diagram of the motor comprises of 3 units: supply source, inverter + motor winding and mechanical system of the drive. The subsystem related to the inverter - motor circuit is shown in Fig. 3.5.

The motor operation is simulated by supplying the winding with a constant voltage source of 24 V throughout the inverter. At a load of T_L = 10 N·m, the following results were obtained: the rotary speed 'n' and source current 'i_s' and phase current 'i_a', which are shown in Fig. 3.6 and Fig. 3.7 respectively. The ripples in the speed waveform are due to the electronic commutation of the transistors. The waveforms of electromotive force (e_a) and armature voltage (V_a) and waveforms of armature current and armature voltage (V_a) are shown in Fig. 3.8 and Fig. 3.9.

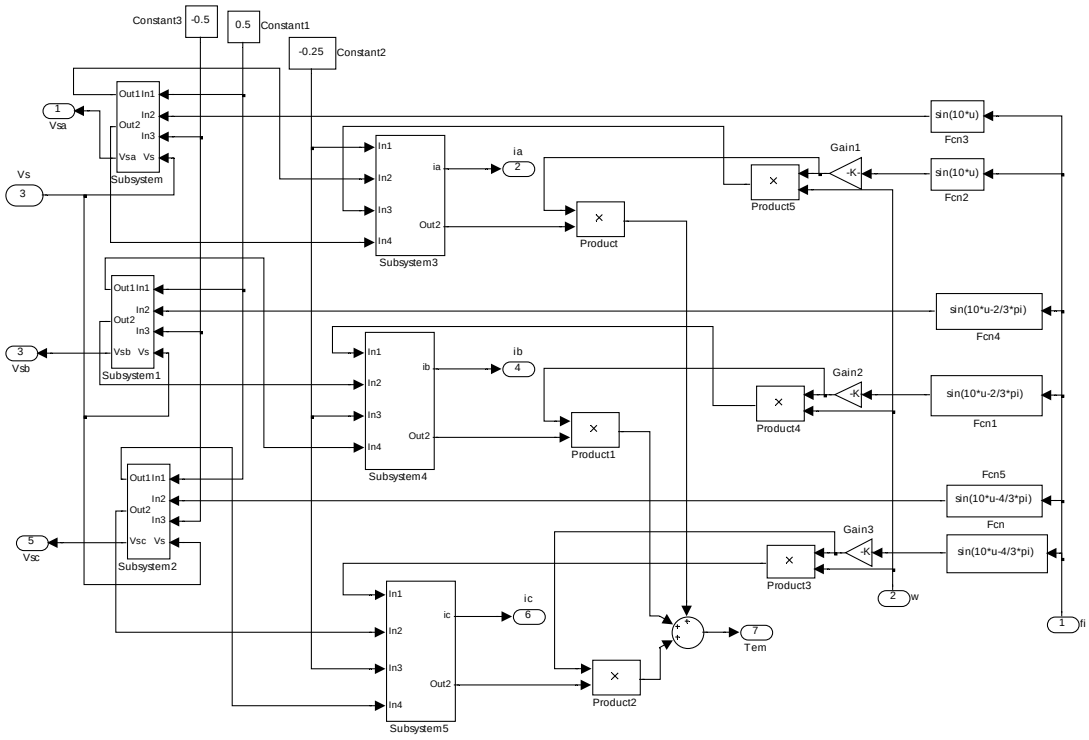

Fig. 3.5 SIMULINK Model of the inverter-motor circuit subsystem

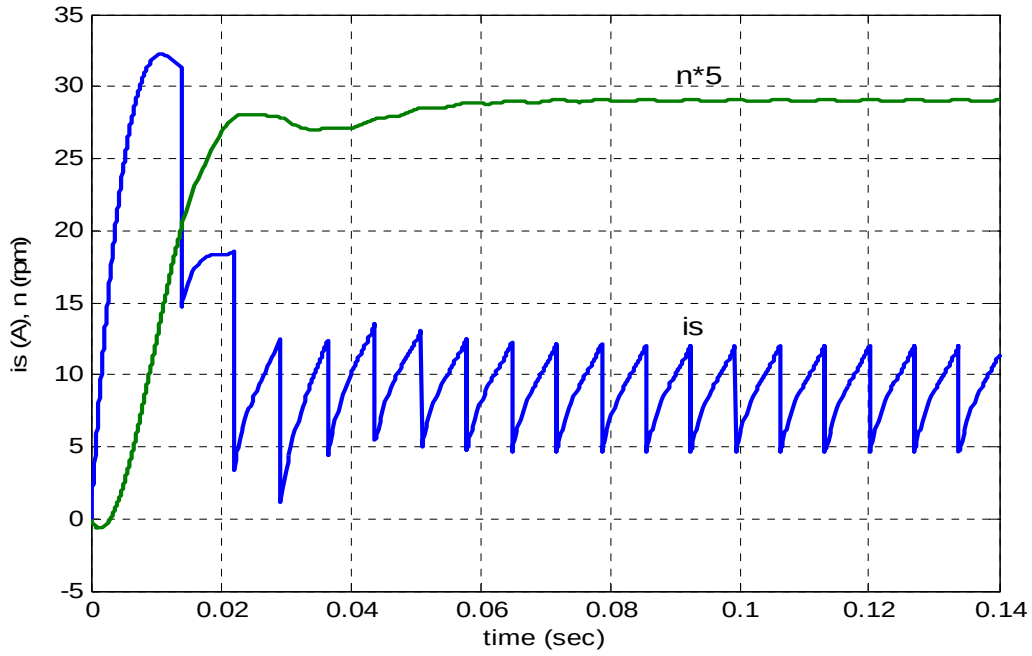

Fig. 3.6 Waveforms of rotary speed and source current

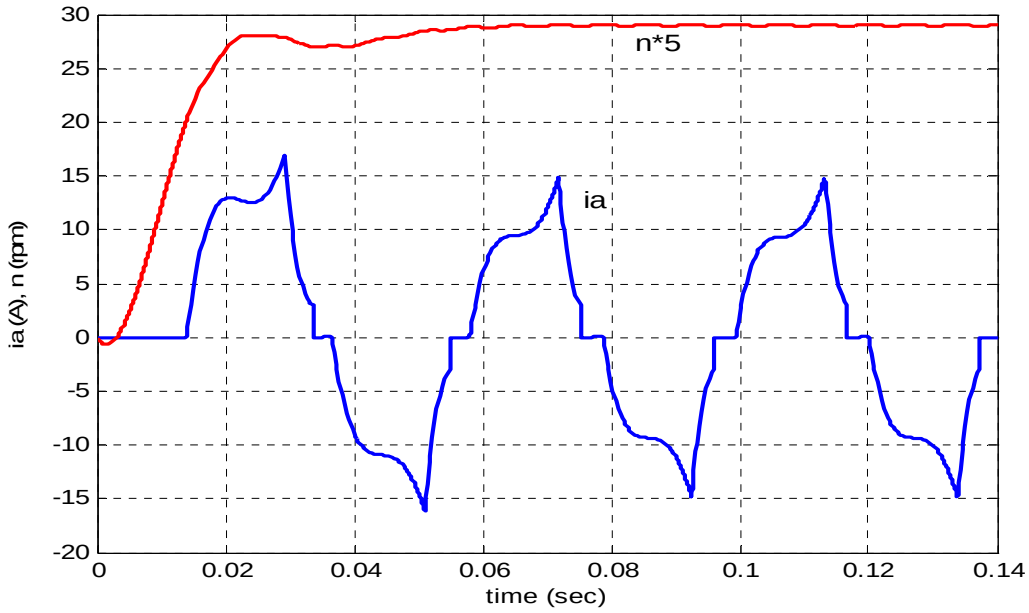

Fig. 3.7 Waveforms of rotary speed and phase current

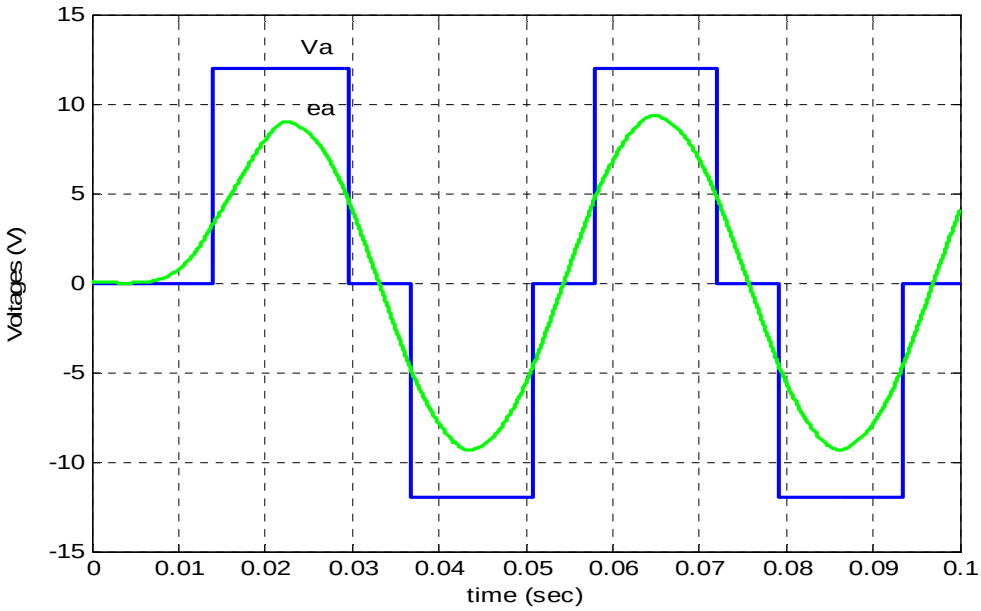

Fig. 3.8 Waveforms of EMF (e_a) and the armature voltage (V_a)

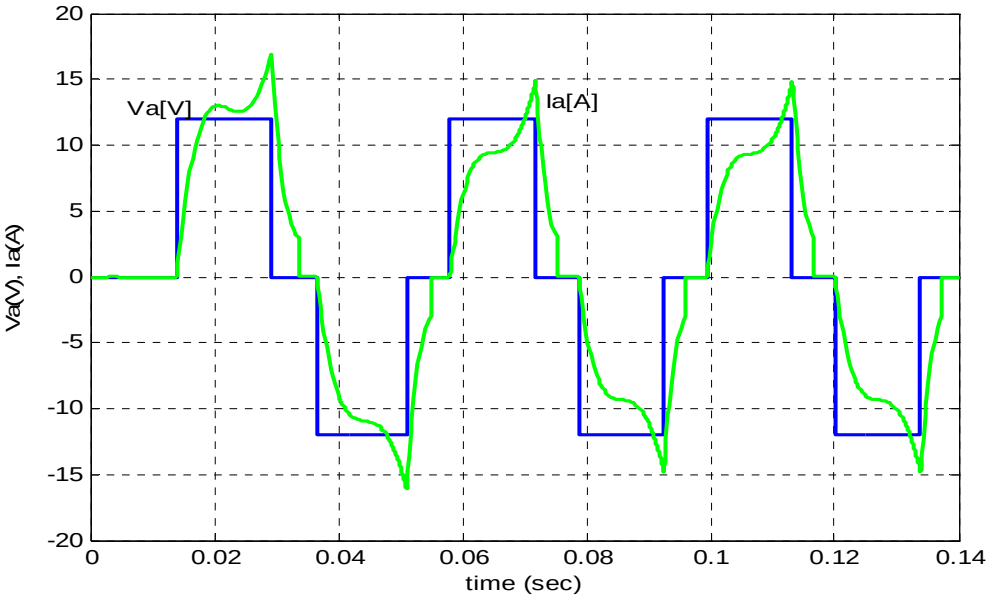

Fig. 3.9 Waveforms of armature current (i_a) and armature voltage (V_a)

The waveforms of electromagnetic torque of the motor (T_{em}) and phase 'a' torque (T_a) are shown in Fig. 3.10. The ripples in the torque are due to the commutation of current in three-phase winding.

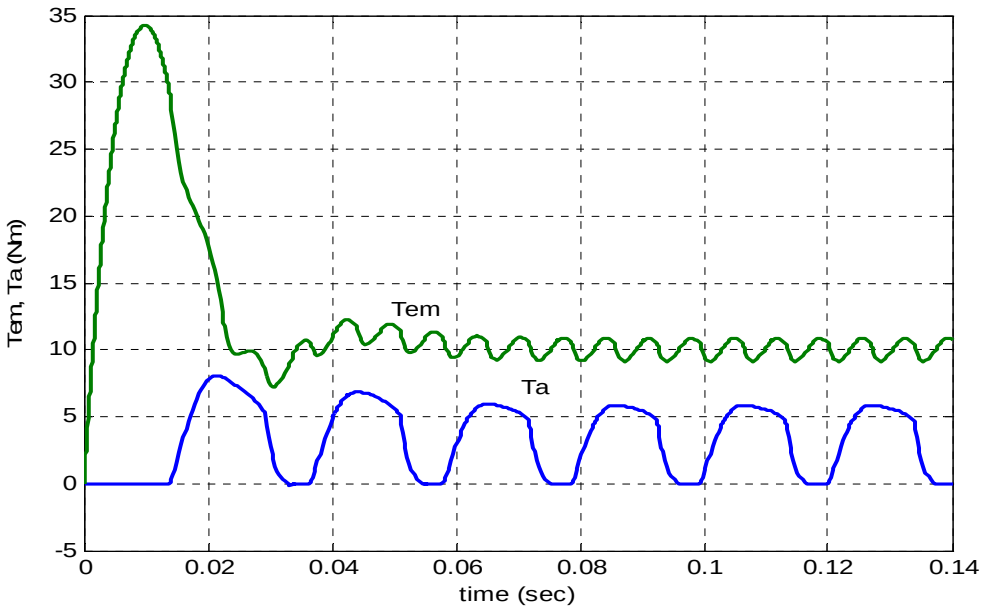

Fig. 3.10 Waveforms of total torque (T_{em}) and phase torque (T_a)

The EMFs induced in the three phases and the armature voltage V_a is shown in Fig. 3.11.

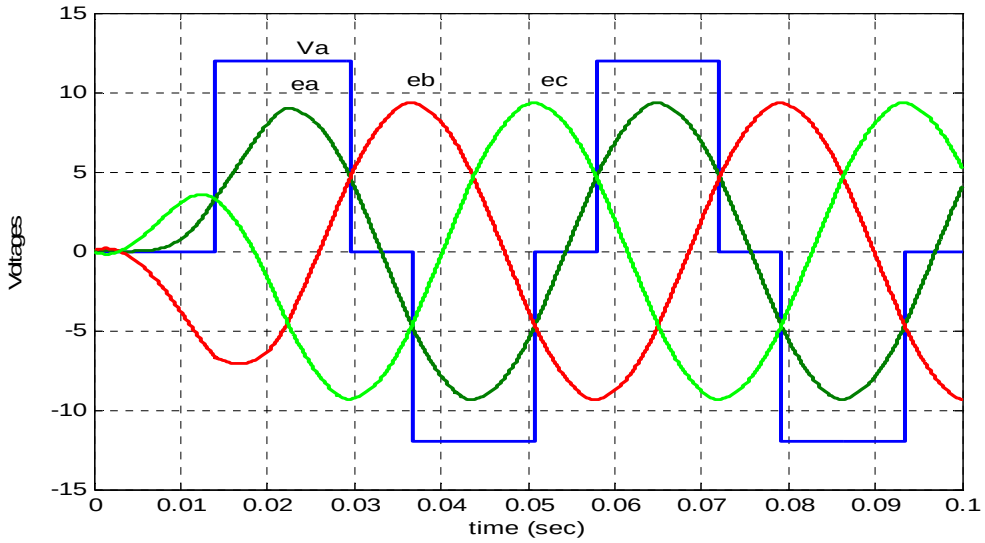

Fig. 3.11 Waveforms of EMFs in the 3phases and the armature voltage (V_a)

3.2 Performance of the Motor in Steady-State Condition

3.2.1 Motor Model for Steady-State Operation

The BLDC motors differ from the conventional brush DC motors by the type of commutator. The latter ones have the mechanical commutator. The winding of BLDC motors are commutated electronically. It means, the analysis of BLDC motor in steady-state conditions can be done by using the brush DC motor model that is shown in Fig. 3.12.

The equations, which describe the motor model, are as follows:

$$T_{em} = K \cdot I \tag{3.29}$$

$$E = K \cdot \omega_m \tag{3.30}$$

$$V = E + I \cdot R_a \tag{3.31}$$

where,

T_{em} – electromagnetic torque,

E – line-to-line electromotive force,

ω_m – rotor angular speed,

K – constant,

$R_a = 2\ R_{ph}$ - armature resistance,

I – average armature current

V – source voltage.

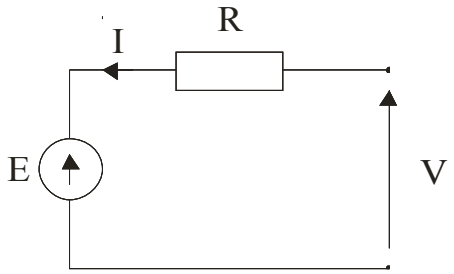

Fig. 3.12 Equivalent circuit of the motor in the steady state conditions

3.2.2 Performance Characteristics of the Motor

The equations of steady-state brush DC motor model written in this section were derived if the inductance of the commutated phase winding doesn't influence the motor operation. This may not be true since 1/3rd of the whole winding (winding of one phase) is commutated at any time, unlikely in brush DC motor where only small portion of the winding is commutated.

For the considered motor, number of magnetic poles, p = 20. The phase inductance of the motor is L_a = 1.75 mH and the phase resistance is R_a = 0.25 Ω. Therefore, at rated speed n = 140 rpm the frequency of the stator current is

$$f = \frac{n \cdot p}{120} = 23.3Hz \tag{3.32}$$

The phase reactance $X_a = 2\pi f L_a = 0.257\Omega$, it means it is equal to the phase resistance. The influence of the inductance of the commutated winding may increase at high speeds. Therefore this influence must be taken into account. It can be done by reducing the flux that induces the voltage E_a in the winding. Thus, the equation for E may be modified in the following way.

$$E = K_f \cdot \Phi \cdot I \cdot \omega_m \tag{3.33}$$

$$E = (C_1 \cdot K + C_2 \cdot I\ ) \cdot \omega_m \tag{3.34}$$

where C_1 and C_2 are constants.

It means, the flux is affected by the current I_a. The constants in the equation (3.34) may be calculated from the electromagnetic characteristics determined from the dynamic simulation in steady-state. The characteristics determined this way are shown in Fig. 3.13. The constants determined on the basis of trial and error method are as follows:

$$K = 1.21,\ C_1 = 0.87,\ C_2 = 0.052.$$

Thus, the electromotive force is equal to

$$\mathrm{E} = (0.87 \cdot K + 0.057 \cdot \mathrm{I}\ )\ \omega_{\mathrm{m}}$$
$$T = K \cdot I$$

The electromechanical characteristics of the motor determined on the basis of the above motor model are shown in Fig. 3.14.

The mechanical power is calculated as follows

$$P_m = T_{em} \cdot \omega_m \tag{3.35}$$

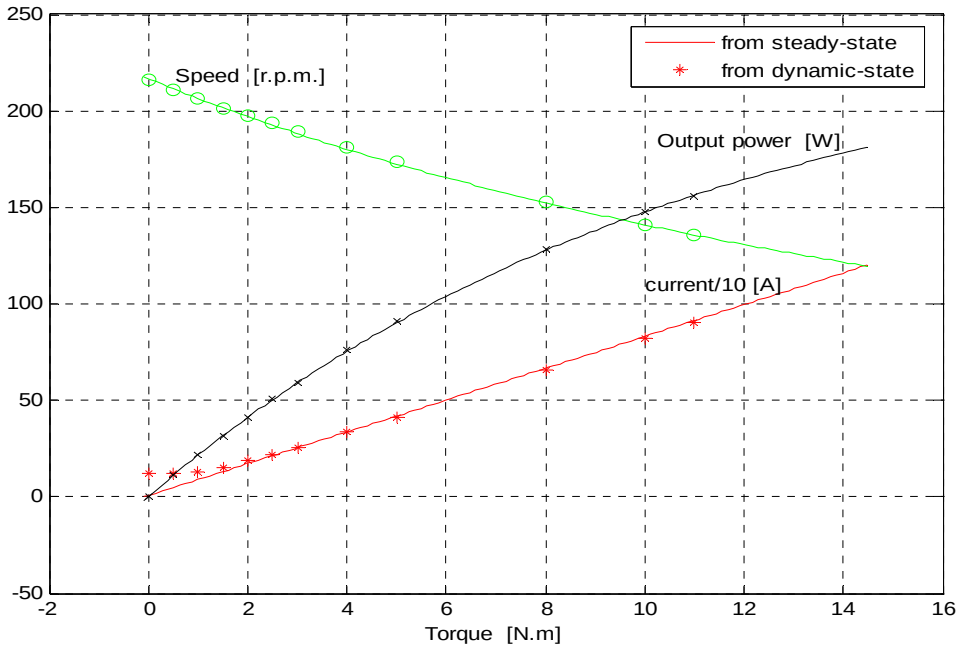

Fig. 3.13 Electromagnetic characteristics determined from the dynamic simulation in steady-state

The efficiency of the motor is

$$Eff_{\%} = \frac{P_{out}}{P_{in}} \cdot 100\% \tag{3.36}$$

where,

$$P_{out} = P_m - \Delta P_m \qquad \text{- output power} \tag{3.37}$$

$$P_{in} = V \cdot I \qquad \text{- input power} \tag{3.38}$$

In calculations, the mechanical power losses were expressed by the equation (3.39)

$$\Delta P_m = \omega_m{}^2 \cdot D \tag{3.39}$$

where D is the friction coefficient of 0.004 *N·m/(rad/s)*

From equations (3.31) and (3.34):

$$\omega = \frac{V - R_a \cdot I}{C_1 \cdot K \ + C_2 \cdot I} \tag{3.40}$$

or

$$\omega_m = \frac{V}{(C_1 \cdot K + C_2 \cdot I\ )} - R_a \left(\frac{T_{em}}{(C_1 \cdot K \ + C_2 \cdot I)^2} \right) \tag{3.41}$$

where,

$$T_{em} = K \cdot I \tag{3.42}$$

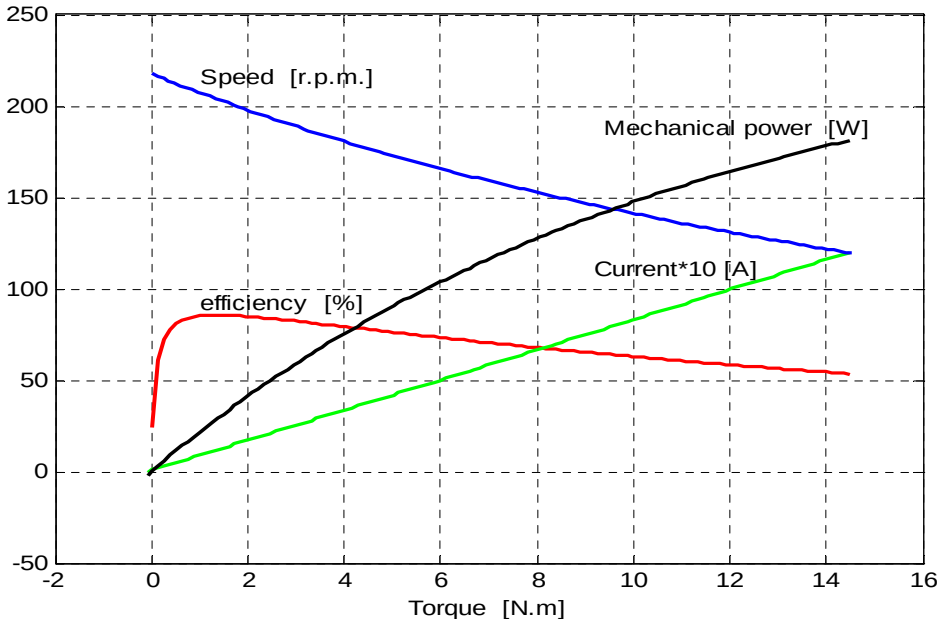

Fig. 3.14 Electromechanical characteristics obtained from steady state model

The motor electromechanical parameters determined from dynamic model and DC brush model for rated supply voltage V = 24 V and rated load torque T_L = 10 N·m are listed in Table 3.2.

Table 3.2 Electromechanical parameters at rated supply and rated load

	Dynamic Model	DC brush model
Supply voltage [V]	24	24
Load torque, T_L [N·m]	10	10
DC current, I_a [A]	8.25	8.3
Rated speed, n [r.p.m]	140.85	141.1
Mechanical power, Pem [W]	147.5	147.5
Input power, P_{in} [W]	230	234.3
Efficiency [%]	64.13	64.93

From above results, the two models (dynamic and steady-state models) produce nearly the same values.

3.3 Influence of Switching Angle of Inverter Transistors on Motor Performance

One of the main factors which influence the performance of the motor is the switching angle 'β'. Fig. 3.15 shows the illustration of the switching angle operation. By changing the switching angle, the efficiency could be varied greatly. The simulation of the motor in section 3.3 was carried out at switching angle $\beta = 0°$.

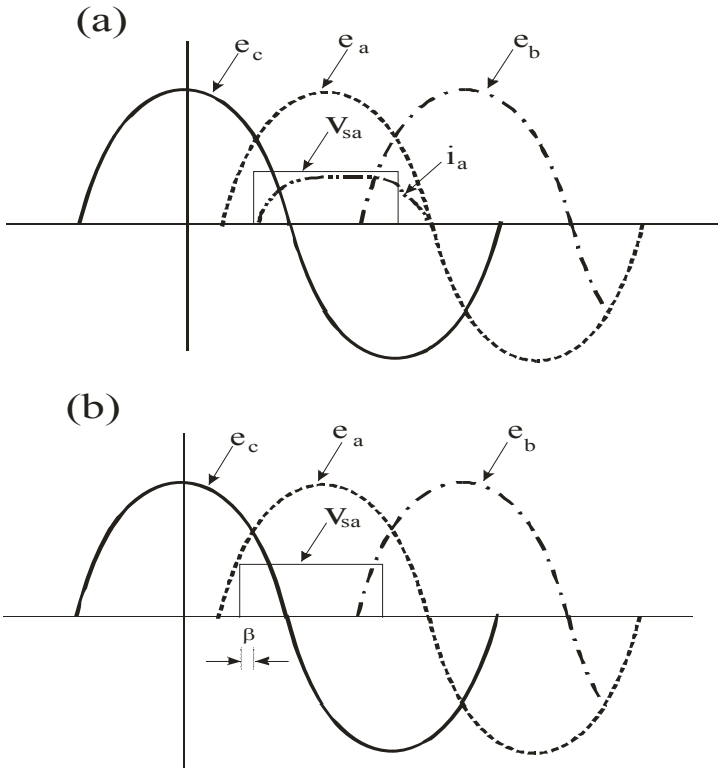

Fig. 3.15 Illustration of the switching angle β (a) zero switching angle (b) switching angle β

To examine the influence on motor performance the simulation was carried out for the following switching angles β = +20°, +10°, 0°, -10°, -20°. The simulation results were plotted in the form of performance characteristics of mean values of input current (i_s), output power (P_m) and efficiency (Eff) and are shown in Figs. 3.16, 3.17, 3.18.

The efficiency was calculated as

$$Eff_{\%} = \frac{P_{out}}{P_{in}}.100\% \tag{3.43}$$

where

$$P_{in} = \frac{1}{T}\int_0^T (v_s \cdot i_{ak})dt \tag{3.44}$$

$$P_{out} = \frac{1}{T}\int_0^T (T_L \cdot \omega)dt \tag{3.45}$$

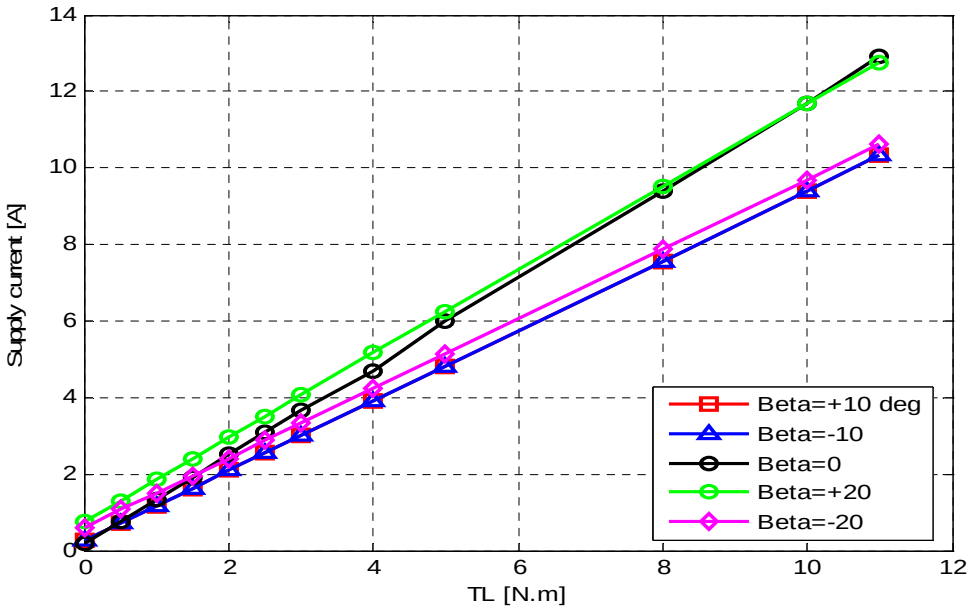

Fig. 3.16 Supply current (i_s) vs load torque (T_L)

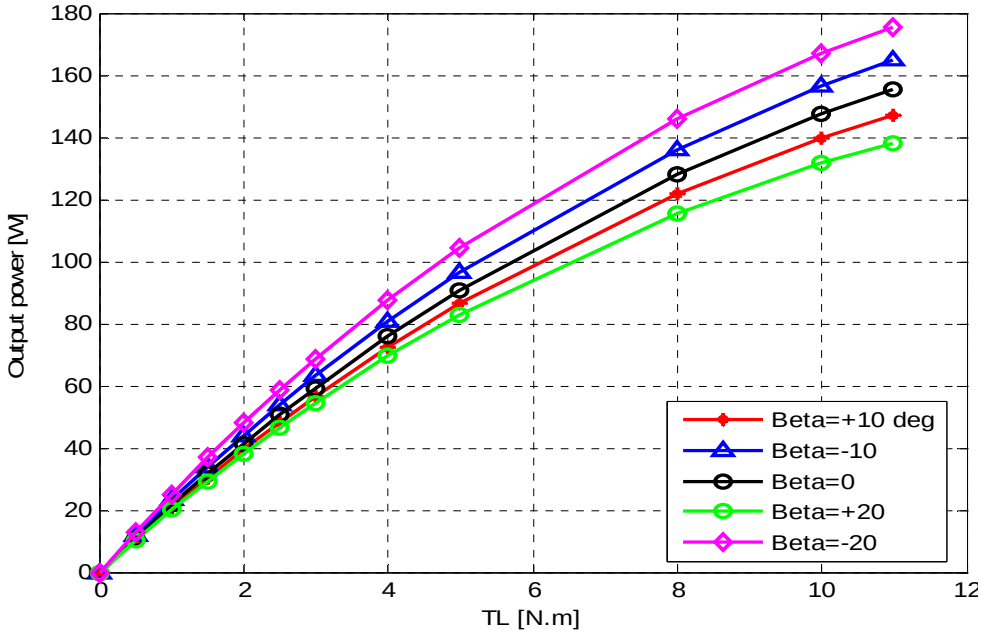

Fig. 3.17 Output power (P_m) vs load torque (T_L)

The characteristics are similar to that of a shunt DC motor or a separately excited DC motor with no armature reaction on the magnetic field of magnets even at high currents which is indicated by the straight line characteristic of current vs torque plot [10]. The magnetic flux is constant, predominated by the magnetic field of the permanent magnets. The current-torque characteristic is shown in Fig 3.16. The speed decreases as the current increases showing that the speed is directly proportional to the induced EMF. The electromechanical power is directly proportional to the input current, since the magnetic flux is constant. The electromagnetic power depends only on the armature current since the magnetic flux is constant. The motor efficiency is maximum when the switching angle β = -10°, which means transistors are switched earlier and the motor efficiency is minimum when β = +20°. This is shown in Fig. 3.18.

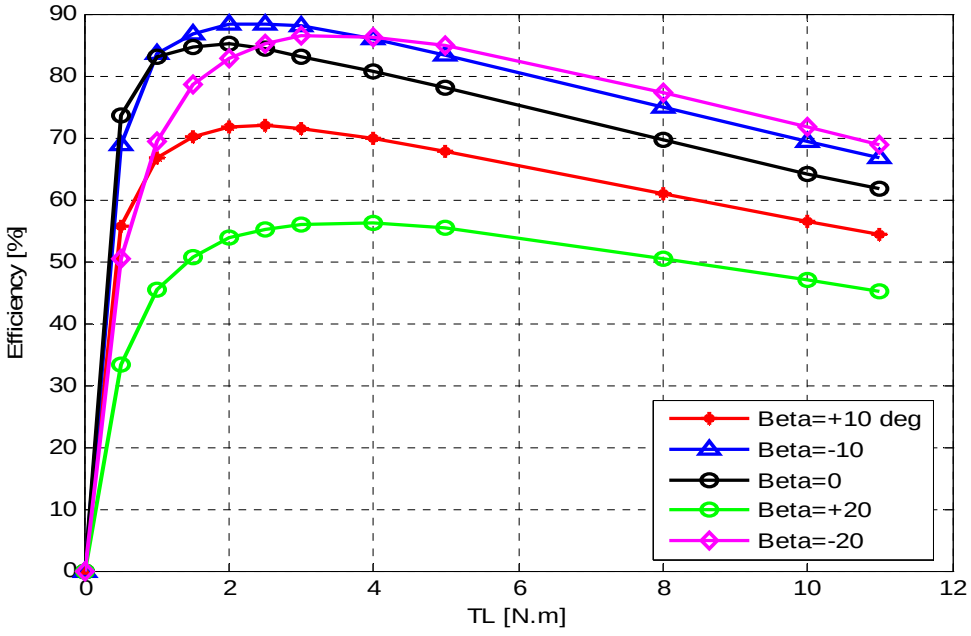

Fig. 3.18 Efficiency (*Eff*) vs load torque (T_L)

The performance characteristics for the switching angle β = -10°, where the efficiency is maximum is shown in Fig. 3.19.

When the motor is loaded heavily, the speed-torque characteristics are almost a straight line and the winding inductance, at heavy loads, can be neglected. The mechanical power output depends on the electromagnetic torque and speed. The electromagnetic torque is directly proportional to the armature current.

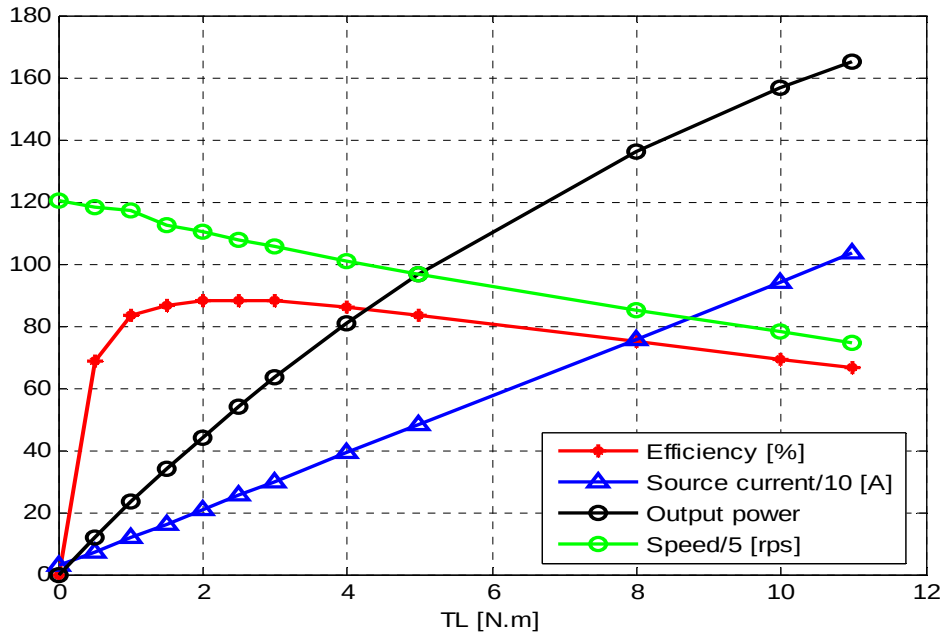

Fig. 3.19 Electromechanical characteristics of the motor for β = -10°

The efficiency of the motor is maximum when the firing angle β = -10° which implies that the transistors were switched on earlier. The efficiency of the motor is minimum when β = +20°, which implies that the switching time of the transistors are delayed.

Chapter 4 : Performance of Torus Motor with the Winding Connected In Two - Phase System

4.1 Analysis in Dynamic Conditions

4.1.1 Dynamic Model of the Motor

The BLDC motor is supplied from a battery through the inverter. The dynamic model of this system is shown in Fig. 4.1. It is derived under the similar assumptions which were considered to derive the dynamic model of the three phase motor in section 3.1.

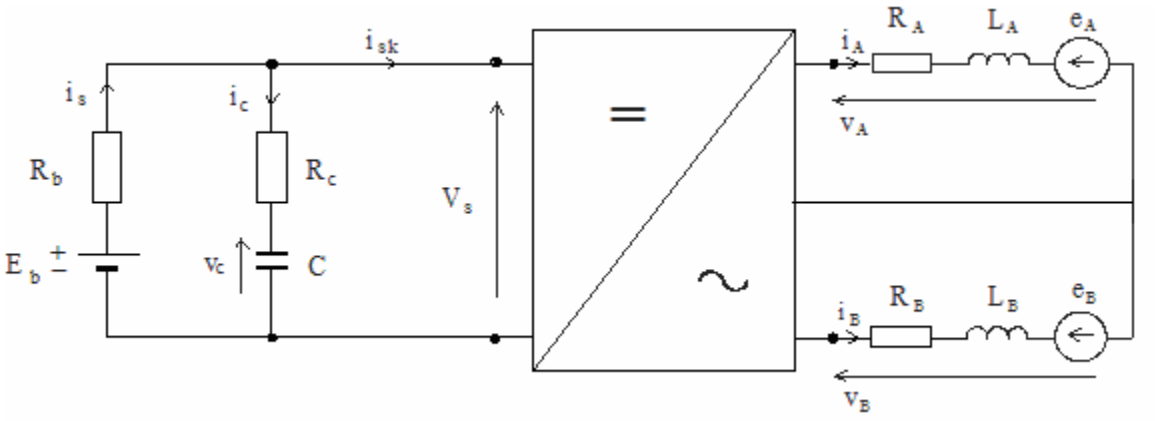

Fig. 4.1 Circuit diagram of supply-inverter-motor system

The equations that describe the model are as follows:

Voltage equations:

- Voltage equations at the source side are the same as for motor with three-phase winding.

- Voltage equations at the motor side (Fig 4.2) are:

$$v_A = v_{sA}$$
$$v_B = v_{sB} \tag{4.1}$$

where:

v_{sA}, v_{sB}, are the inverter output voltages that supply the two – phase winding

v_A, v_B, are the voltages across the motor armature winding.

v_N – voltage at the neutral point.

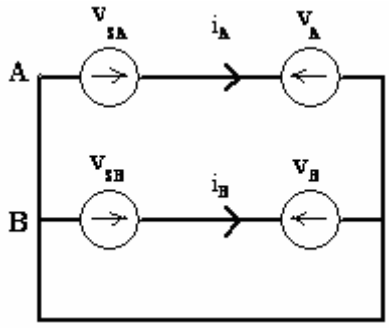

Fig. 4.2 Scheme to equation 4.1

The equation of the voltages across the motor winding

$$\begin{bmatrix} v_A \\ v_B \end{bmatrix} = \begin{bmatrix} R_a & 0 \\ 0 & R_b \end{bmatrix} \begin{bmatrix} i_A \\ i_B \end{bmatrix} + \frac{d}{dt} \begin{bmatrix} L_A & L_{AB} \\ L_{BA} & L_B \end{bmatrix} \begin{bmatrix} i_A \\ i_B \end{bmatrix} + \begin{bmatrix} e_A \\ e_B \end{bmatrix} \tag{4.2}$$

or in shorter version:

$$\mathbf{V_a} = \mathbf{R_a} \cdot \mathbf{I_a} + \frac{\mathbf{d}}{\mathbf{dt}} \mathbf{L_a} \cdot \mathbf{I_a} + \mathbf{E_a} \tag{4.3}$$

Since the resistances R_a of all phases are the same:

$$\mathbf{R_a} = \begin{bmatrix} R_a & 0 \\ 0 & R_a \end{bmatrix} \tag{4.4}$$

Since, the phases A and B are displaced by 90° in space, there is no mutual inductance between the phases A and B. Therefore,

$$L_{AB} = L_{BA} = 0 \tag{4.5}$$

Due to the symmetrical winding the inductances

$$L_A = L_B = L \tag{4.6}$$

The inductance matrix takes the form:

$$L_a = \begin{bmatrix} L & 0 \\ 0 & L \end{bmatrix} \tag{4.7}$$

With respect to equations 4.4 and 4.7, the voltage equation takes the form:

$$\begin{bmatrix} v_A \\ v_B \end{bmatrix} = \begin{bmatrix} R_A & 0 \\ 0 & R_B \end{bmatrix} \begin{bmatrix} i_A \\ i_B \end{bmatrix} + \frac{d}{dt} \begin{bmatrix} L & 0 \\ 0 & L \end{bmatrix} \begin{bmatrix} i_A \\ i_B \end{bmatrix} + \begin{bmatrix} e_A \\ e_B \end{bmatrix} \tag{4.8}$$

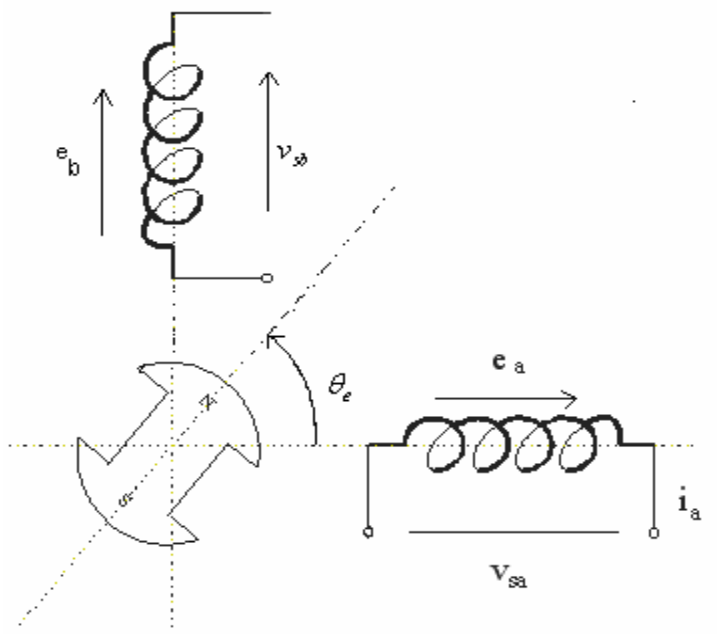

Fig. 4.3 Position of the rotor with respect to the phase 'A'

The electromotive force induced in the phase '*A*' winding (see Fig 4.3):

$$e_a = K_E \omega_m \sin\theta_e \tag{4.9}$$

The electromotive force induced in the phase *B* winding is given by

$$e_b = K_E \omega_m \sin(\theta_e - 90^0) \tag{4.10}$$

where:

K_E – constant

ω_m – rotor angular speed:

$$\omega_m = \frac{1}{p}\frac{d\theta_e}{dt} \tag{4.11}$$

θ_e – electrical angle (Fig 4.3)

p – number of pole pairs

For three-phase winding, the electromotive forces written in a form of matrix $\boldsymbol{E_a}$

$$\mathbf{E_a} = \frac{K_E}{p}\begin{bmatrix} \sin\theta_e \\ \sin(\theta_e - \frac{\pi}{2}) \end{bmatrix}\frac{d\theta_e}{dt} \tag{4.12}$$

Equation that links the supply and motor sides:

$$i_{sk} = \frac{1}{v_s}(i_A v_{sA} + i_B v_{sB}) \tag{4.13}$$

which is derived from the equality of the powers at input and output of the inverter.

Supply voltages for the phases (v_{sA}, v_{sB}) results from the operation of converter.

Motion equations:

Electromagnetic torque for two-phase is given by following equations:

$$T_{em} = \frac{e_A i_A}{\omega_m} + \frac{e_B i_B}{\omega_m} \tag{4.14}$$

$$T_{em} = \frac{e_A i_A}{\omega_m} + \frac{e_B i_B}{\omega_m} = K_E(f_a(\theta_e) \cdot i_A + fb(\theta_e) \cdot i_B) \tag{4.15}$$

where

$$f_a(\theta_e) = \sin(\theta_e)$$
$$f_b(\theta_e) = \sin(\theta_e - \frac{\pi}{2})$$

Combining all the above equations, the system in steady-space form is

$$\dot{x} = Ax + Bu \tag{4.16}$$

$$x = \begin{bmatrix} i_A & i_B & \omega_m & \theta_e \end{bmatrix}^t \tag{4.17}$$

$$A = \begin{bmatrix} -\frac{R_s}{L} & 0 & -\frac{K_E(f_a(\theta_e))}{L} & 0 \\ 0 & -\frac{R_s}{L} & -\frac{K_E(f_a(\theta_e))}{L} & 0 \\ \frac{K_E(f_a(\theta_e))}{J} & \frac{K_E(f_b(\theta_e))}{J} & -\frac{D}{J} & 0 \\ 0 & 0 & \frac{P}{2} & 0 \end{bmatrix} \tag{4.18}$$

$$B = \begin{bmatrix} \frac{1}{L} & 0 & 0 \\ 0 & \frac{1}{L} & 0 \\ 0 & 0 & -\frac{1}{J} \\ 0 & 0 & 0 \end{bmatrix} \tag{4.19}$$

$$u = \begin{bmatrix} v_A & v_B & T_L \end{bmatrix}^t \tag{4.20}$$

4.1.2 Parameters of Electrical Circuit and Mechanical System

The two-phase inverter is supplied from the same power source as it was for three-phase motor. Since the same coils of motor were connected in two-phase system (see Fig. 2.18) the resistance and inductance of two-phase relate to the resistance and inductance of three-phase winding in the following way:

Number of magnetic poles, p = 30

Phase resistance

$$R_{2ph} = \frac{N_{c/ph}^{2ph}}{N_{c/ph}^{3ph}} R_{3ph} = \frac{30}{20} 0.25 = 0.375\ \Omega \tag{4.21}$$

Leakage inductance per phase

$$L_l^{2ph} = \left(\frac{N_{c/ph}^{2ph}}{N_{c/ph}^{3ph}} \right)^2 L_l^{3ph} = \left(\frac{30}{20} \right)^2 0.1 = 0.225\ mH \tag{4.22}$$

Single phase magnetizing inductance

$$L_m^{2ph} = \left(\frac{N_{c/ph}^{2ph}}{N_{c/ph}^{3ph}} \right)^2 L_{1-phase,m}^{3ph} = \left(\frac{N_{c/ph}^{2ph}}{N_{c/ph}^{3ph}} \right)^2 \frac{2}{3} L_m^{3ph} = \left(\frac{30}{20} \right)^2 \frac{2}{3} \cdot 1.1 = 1.32\ mH \tag{4.23}$$

Self inductance

$$L^{2ph} = L_l^{2ph} + L_m^{2ph} = 0.225 + 1.32 = 1.545\ mH \tag{4.24}$$

EMF coefficient (per phase for AC representation)

$$K_{E_m}^{2ph} = \frac{N_{c/ph}^{2ph}}{N_{c/ph}^{3ph}} K_{E_m}^{2ph} = \frac{30}{20} 0.628 = 0.942\ \frac{V}{rad/s} \tag{4.25}$$

The parameters of electrical and mechanical system are given below in Table 4.1. A two-phase motor doesn't have any mutual inductance. It has only leakage and magnetizing inductance.

Table 4.1 Parameters of the electrical and mechanical system

Parameters of the supply system:	
EMF of the battery	$E_b = 24\ V$
Source resistance	$R_s = 0.0005\ \Omega$
Resistance in series with capacitor	$R_c = 10\ \Omega$
Capacitance	$C = 0.00001\ F$
Parameters of the motor circuit:	
Phase resistance of the brushless DC motor	$R_a = 0.375\ \Omega$
Leakage inductance per phase	$L_l = 0.225mH$
Magnetizing inductance	$L_m = 1.32mH$
Self inductance of the DC brushless motor	$L_a = L_l + L_m = 1.545mH$
EMF constant	$K_e = E_m / \omega_m = 0.942\ V/ (rad/s)$
Parameters of the mechanical system:	
Moment of inertia	$J = 0.021\ Kg/m^2$
Friction coefficient	$D = 0.004\ N{\cdot}m/ (rad/s)$
Load torque	$T_{load} = 10N{\cdot}m$

4.1.3 Simulation of Motor Dynamics

The block diagram of the motor is built using MATLAB/SIMULINK in accordance with the mathematical model derived in section 4.1. The block diagram of the model is shown in Fig. 4.4.

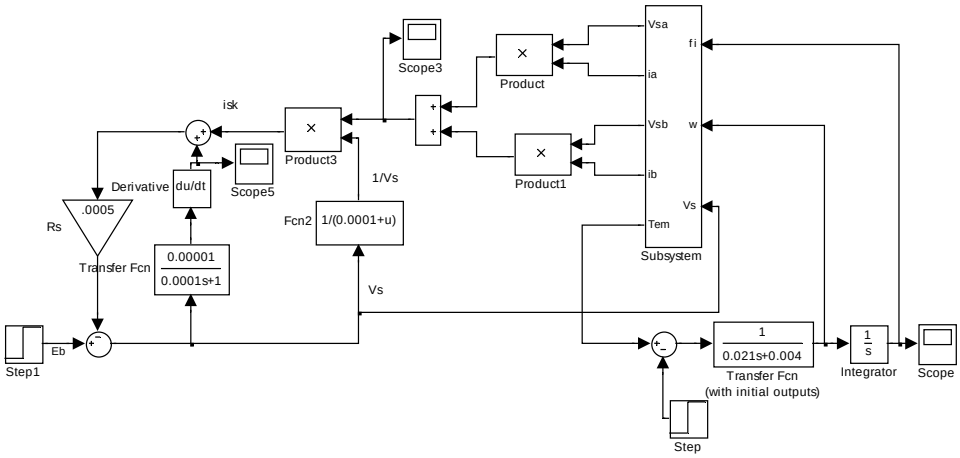

Fig. 4.4 SIMULINK model of two-phase brushless DC motor

The main block diagram of the motor comprises of 3 units: supply source, inverter + motor winding and mechanical system of the drive. The subsystem related to the inverter motor circuit is shown in Fig. 4.5.

The motor operation is simulated by supplying the winding with a constant voltage source of 24 V throughout the inverter. The results of simulation in which the motor was starting being loaded by the torque T_L = 10 N·m are shown in Fig. 4.6 through Fig. 4.11.

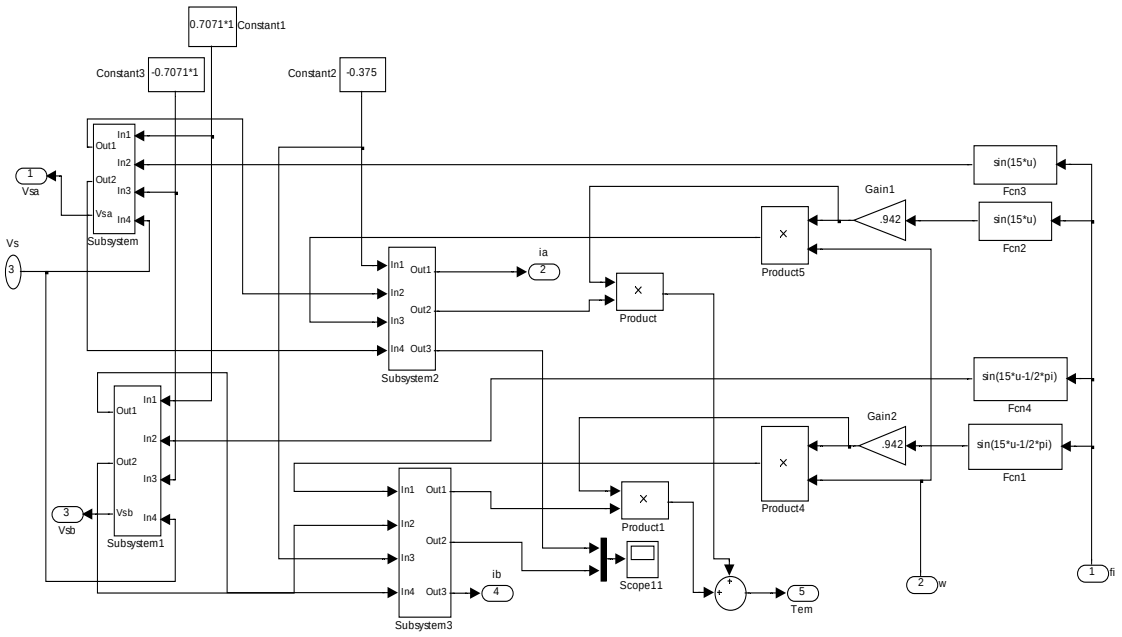

Fig. 4.5 SIMULINK model of the inverter-motor circuit subsystem

Fig. 4.6 and Fig. 4.7 show the waveforms of the rotary speed 'n', source current 'i_s' and phase 'a' current 'i_a'. The ripples in the speed waveform are due to the electronic commutation of the transistors. The waveforms of electromotive force (e_a) and supply voltage (v_{sa}) and armature current (i_a) are shown in Fig. 4.8 and Fig. 4.9. The waveforms of electromagnetic torque of the motor (T_{em}) and phase torque (T_{ema}) are in shown in Fig. 4.10. The ripples in the torque are due to the winding commutation. The EMFs induced in the three phases and the supply voltage v_{sa} are shown in Fig. 4.11.

With the similar discussion, carried out in section 3.4.2, the equations which describe the two-phase motor model are as follows:

$$T = K \cdot I - B \cdot \omega_m \tag{4.26}$$

where K and B are constants.

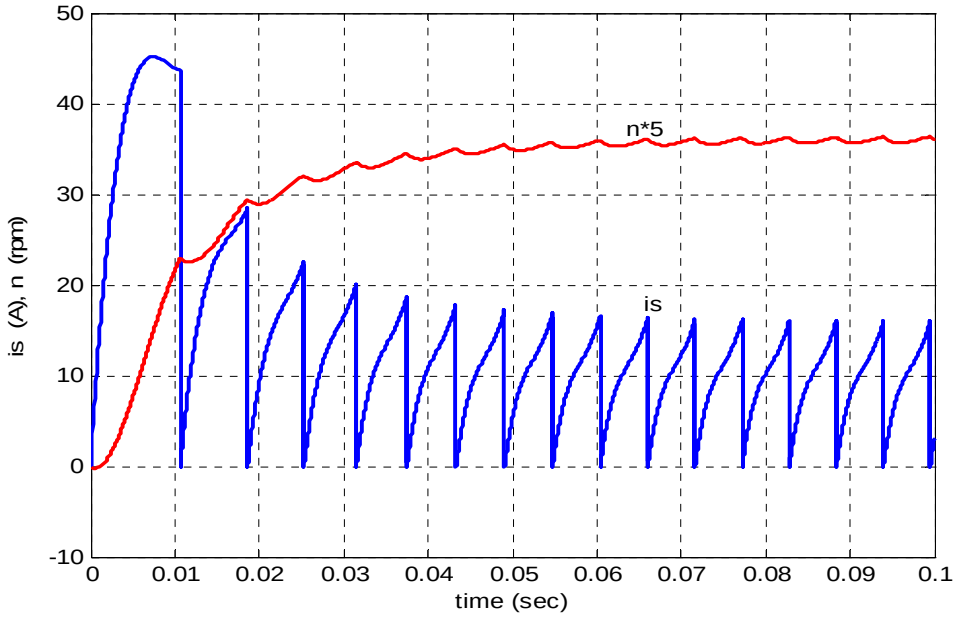

Fig. 4.6 Waveform of rotary speed and source current

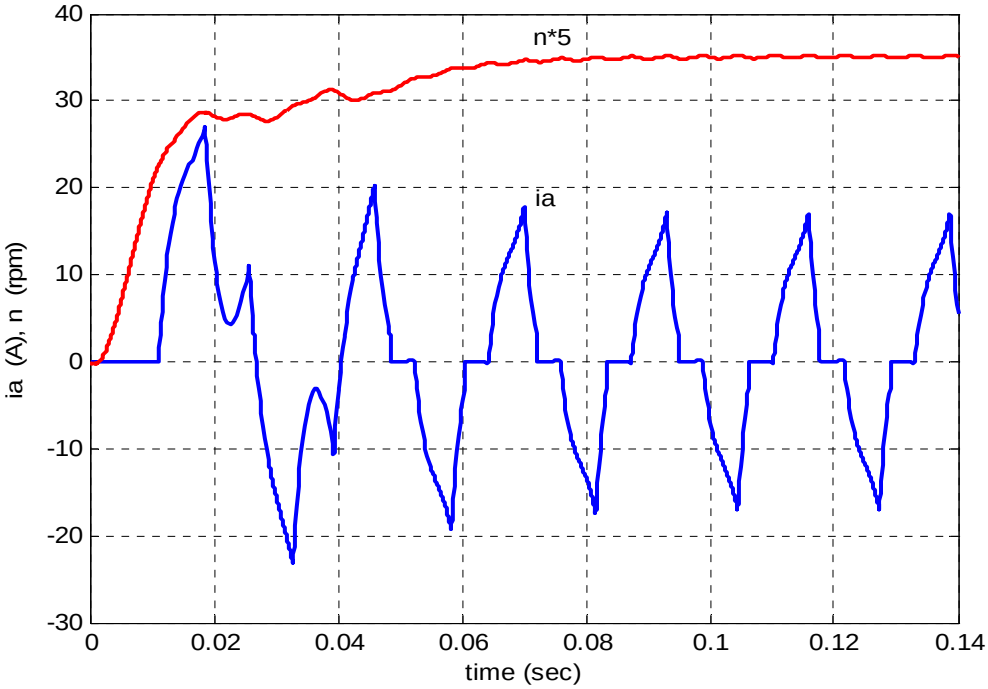

Fig. 4.7 Waveform of rotary speed and phase current

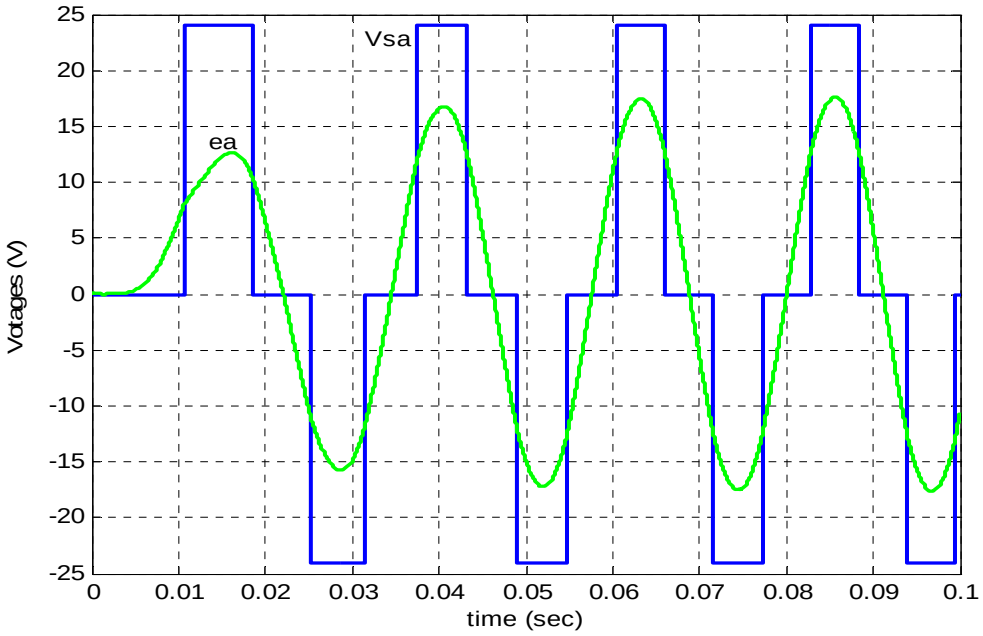

Fig. 4.8 Waveform of EMF (e_a) and the armature voltage (V_{sa})

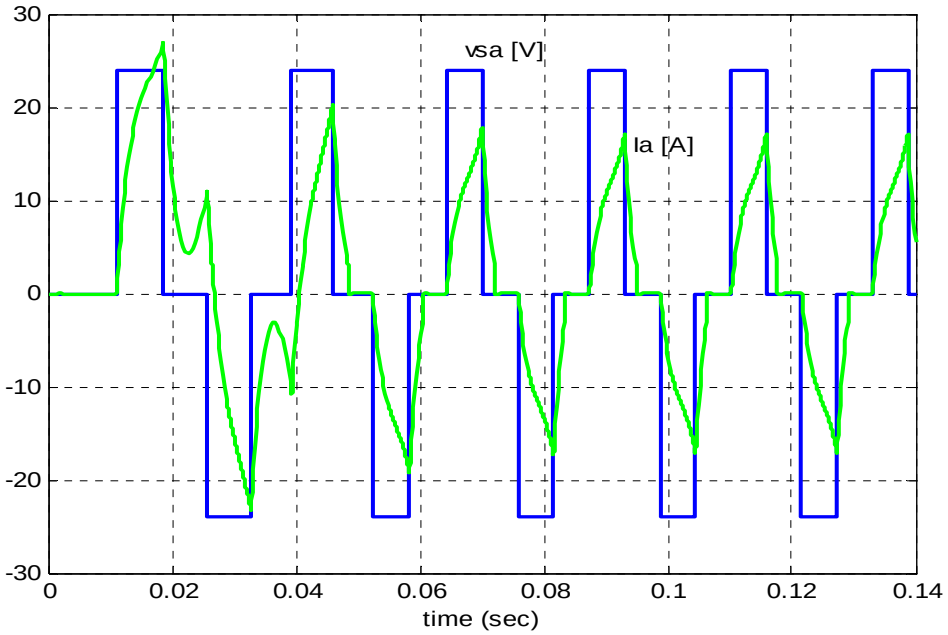

Fig. 4.9 Waveforms of armature current (i_a) and supply voltage (v_{sa})

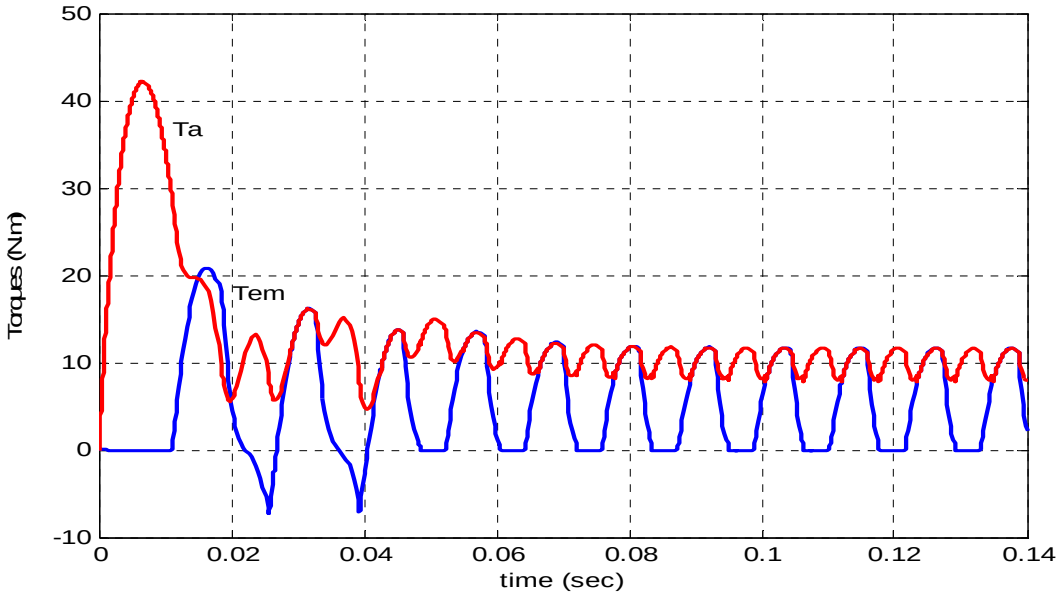

Fig. 4.10 Waveforms of total torque (T_{em}) and phase torque (T_a)

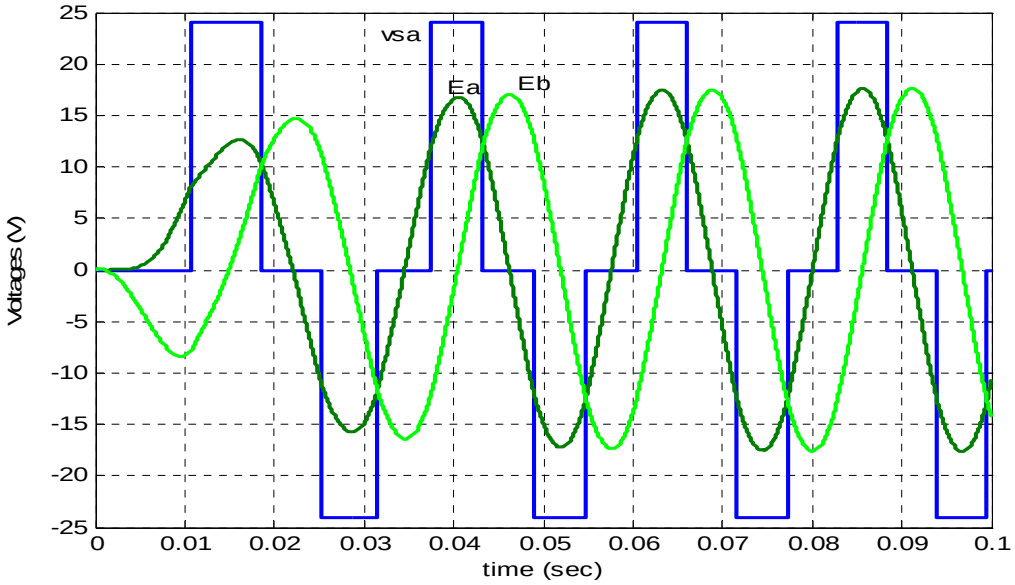

Fig. 4.11 Waveforms of EMFs in the two phases and the supply voltage (v_{sa})

$$E_a = (C_1 \cdot K_E + C_2 \cdot I_a) \cdot \omega_m \tag{4.27}$$

where C_1 and C_2 are constants.

It means the flux is affected by the current 'I'. The constants in the equation (4.27) may be calculated from the electromagnetic characteristics determined from the dynamic simulation in steady-state. The characteristics determined this way are shown in Fig. 4.12.

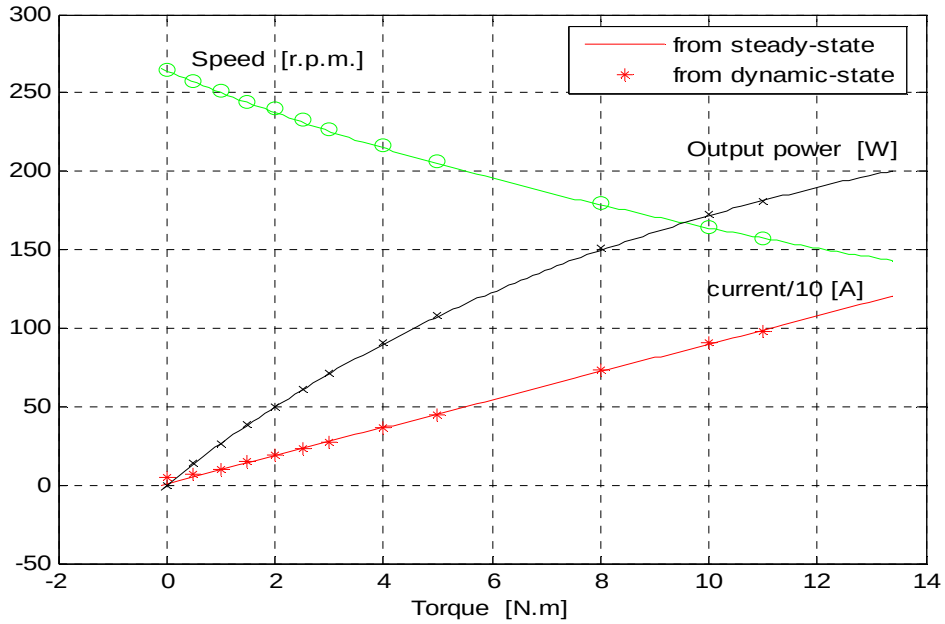

Fig. 4.12 Electromagnetic characteristics determined from the dynamic simulation in steady-state

The constants determined on the basis of trial and error method are as follows:

$$K = 1.12,\ C_1 = 0.77,\ C_2 = 0.045.$$

Thus, the electromotive force is equal to

$$\mathrm{E} = (0.77 \cdot K + 0.045 \cdot \mathrm{I})\,\omega_{\mathrm{m}}$$

$$T = K \cdot I$$

The electromechanical characteristics of the motor determined on the basis of the above motor model are shown in Fig. 4.13.

The mechanical power is calculated as follows

$$P_m = T_{em} \cdot \omega_m \tag{4.28}$$

The efficiency of the motor is

$$Eff_{\%} = \frac{P_{out}}{P_{in}} \cdot 100\% \tag{4.29}$$

where,

$$P_{out} = P_m - \Delta P_m \qquad \text{- output power} \tag{4.30}$$

$$P_{in} = V \cdot I_a \qquad \text{- input power} \tag{4.31}$$

In calculations, the mechanical power losses were expressed by the equation (4.32)

$$\Delta P_m = \omega_m{}^2 \cdot D \tag{4.32}$$

where D is the friction coefficient of 0.004 *N·m/(rad/s)*

Therefore,

$$\omega = \frac{V - R_a \cdot I}{C_1 \cdot K \ + C_2 \cdot I} \tag{4.33}$$

or

$$\omega_m = \frac{V}{(C_1 \cdot K + C_2 \cdot I \ )} - R_a \left(\frac{T_{em}}{(C_1 \cdot K \ + C_2 \cdot I)^2} \right) \tag{4.34}$$

where,

$$T_{em} = K \cdot I \tag{4.35}$$

The motor electromechanical parameters determined from dynamic model and DC brush model for rated supply voltage V = 24 V and rated load torque T_L = 10 N·m are listed in Table 4.2. From the results listed in Table 4.2, the two models (dynamic and steady-state models) produce nearly the same values.

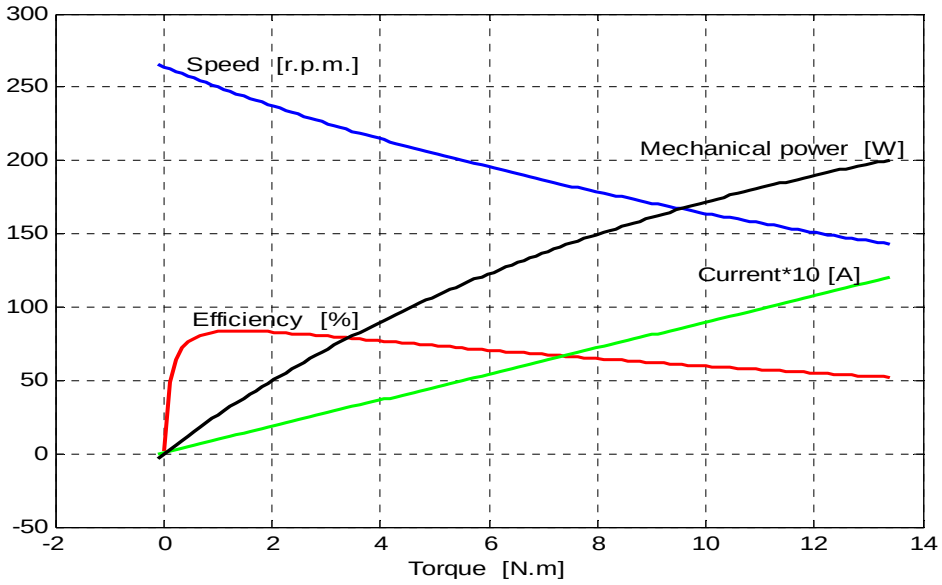

Fig. 4.13 Electromechanical characteristics obtained from steady-state model

4.2 Influence of Switching Angle of Inverter Transistors on Motor Performance

Similarly as for the three-phase BLDC motor, it was examined the influence of switching angle on motor performance. The triggering angles (switching angles) of the transistors are varied and the performance characteristics were plotted.

The calculations were carried out for the following switching angles β = +20°, +10°, 0°, -10°, -20° (see Fig. 4.14). The simulation results were plotted in the form of performance characteristics of mean values of input current (i_s), output power (P_m) and efficiency (*Eff*) and are shown in Figs. 4.15, 4.16, 4.17.

The efficiency was calculated as

$$Eff_{\%} = \frac{P_{out}}{P_{in}}.100\% \qquad (4.36)$$

Table 4.2 Electromechanical parameters at rated supply and rated load

	Dynamic Model	DC brush model
Supply voltage [V]	24	24
Load torque, T_L [N·m]	10	10
DC current, I_a [A]	9.1	9.0
Rated speed, n [r.p.m]	164.44	141.1
Mechanical power, Pem [W]	172.5	171.8
Input power, P_{in} [W]	281	288
Efficiency [%]	61.39	59.65

where

$$P_{in} = \frac{1}{T}\int_0^T (v_s \cdot i_{ak})dt \tag{4.37}$$

$$P_{out} = \frac{1}{T}\int_0^T (T_L \cdot \omega)dt \tag{4.38}$$

The characteristics are similar to that of a shunt DC motor or a separately excited DC motor with no armature reaction. The magnetic flux is constant, predominated by the magnetic field of the permanent magnets. The current-torque characteristic is shown in Fig 4.15. The speed decreases as the current increases showing that the speed is directly proportional to the induced EMF. The electromechanical power is directly proportional to the input current, since the magnetic flux is constant. The electromagnetic power depends only on the armature current since the magnetic flux is constant. The motor efficiency is

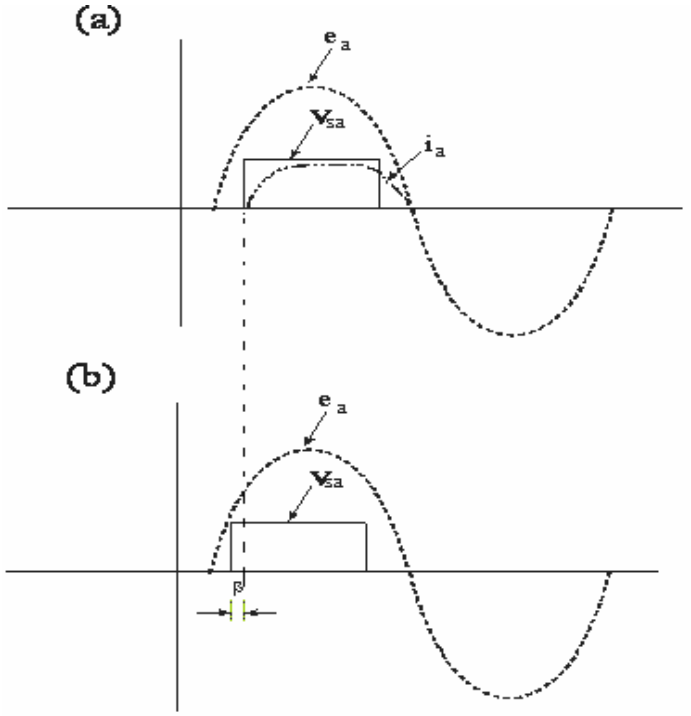

Fig. 4.14 Illustration of the switching angle β (a) zero switching angle (b) switching angle β

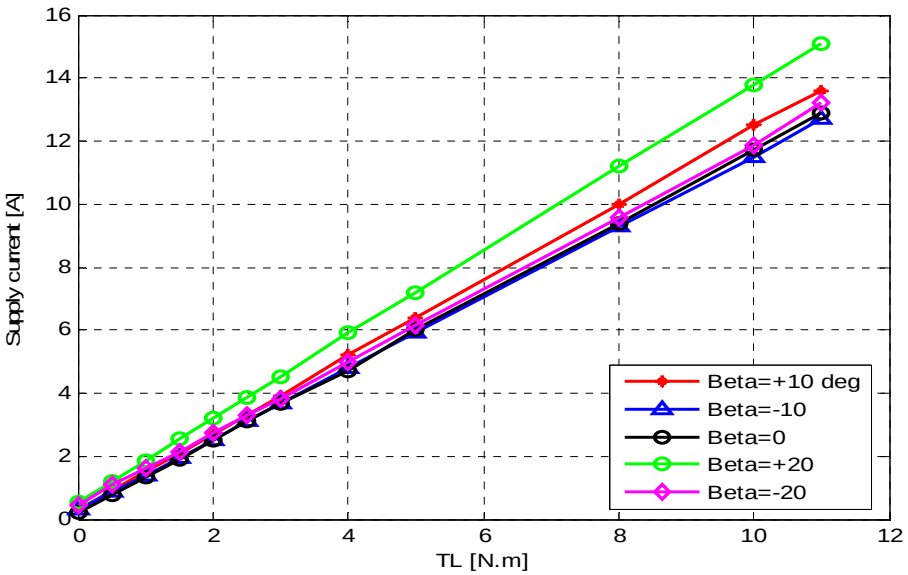

Fig. 4.15 Supply current (i_s) vs load torque (T_L)

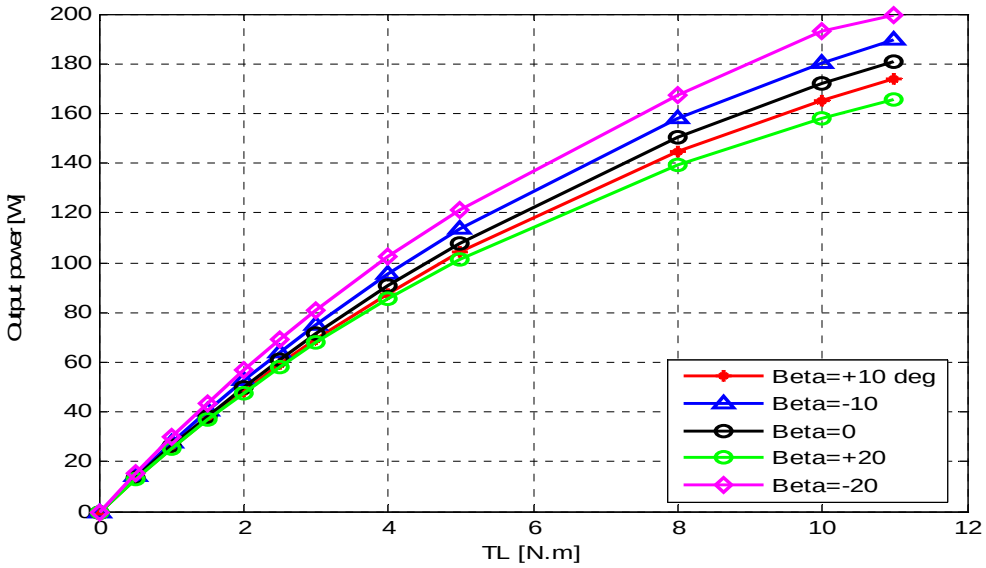

Fig. 4.16 Output power (P_m) vs load torque (T_L)

maximum when the switching angle β = -10°, which means transistors are switched earlier and the motor efficiency is minimum when β = +20°. This is shown in Fig. 4.17. The performance characteristics for the switching angle β = -10°, where the efficiency is maximum is shown in Fig. 4.17. When the motor is loaded heavily, the speed-torque characteristics are almost a straight line and the winding inductance, at heavy loads, can be neglected. The mechanical power output depends on the electromagnetic torque and speed. The electromagnetic torque is directly proportional to the armature current. The efficiency of the motor is maximum when the firing angle β = -10° which implies that the transistors were switched on earlier. The efficiency of the motor is minimum when β = +20°, which implies that the switching time of the transistors are delayed.

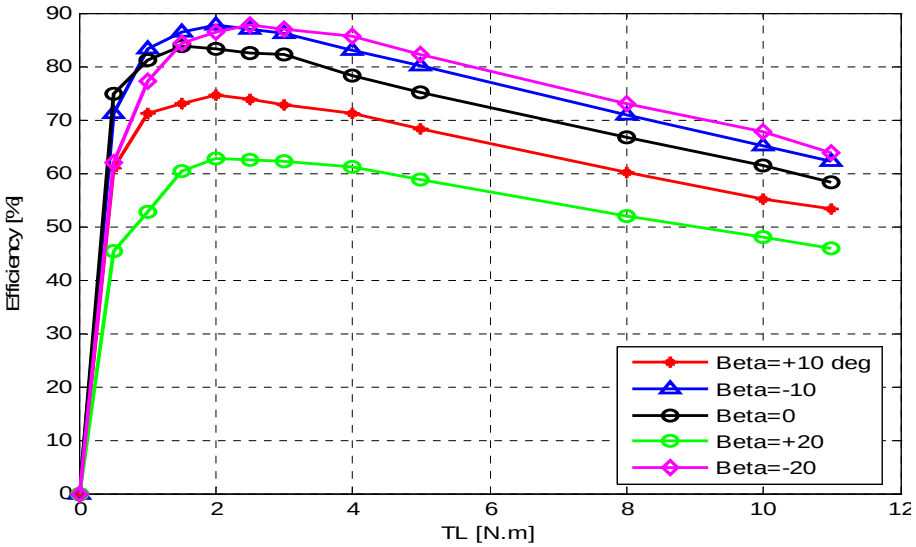

Fig. 4.17 Efficiency (*Eff*) vs load torque (T_L)

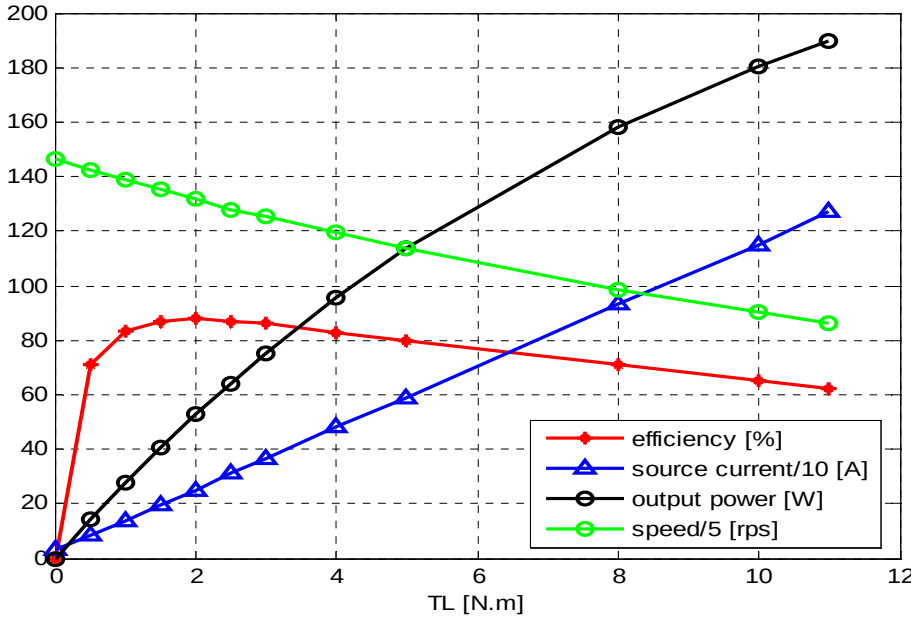

Fig. 4.18 Electromechanical characteristics of the motor for β = -10°

Chapter 5 : Conclusions

The performance of brushless DC motors connected in three-phase and two-phase winding systems were analyzed in this thesis. The analysis of the motors was carried by building the models of source-inverter-motor circuit based upon the electromechanical equations which describes the motor. For simulation of the model block diagrams, the software package MATLAB/SIMULINK was used. Performance of the models in both steady – state and dynamic – state conditions were taken into consideration.

The following conclusions are drawn from the comparative study of the motor connected in three-phase and two-phase systems:

- By having a look at the electromagnetic torque vs. load torque characteristics, the quantity of torque ripples in three-phase system is less when compared to that of in two-phase system. So, the three-phase motor could be used where a smooth ride is the pivotal concern such as in wheelchairs, elevators, etc. By increasing the number of phases in the winding connection of motor, the ripples in the torque could be reduced greatly. But by the increasing the number of phases, the inverter circuit becomes complex to design and also it increases the manufacturing costs.
- Observing the electromechanical characteristics, the two motors have similar kind of characteristics. But the performance parameters like the maximum speed, maximum torque, mechanical output power, rated current, efficiency etc. are different.

- Comparing the electromechanical characteristics, we could see that the maximum efficiency in three-phase system is 85.17 % at 2 N·m and that of 83.3 % in two-phase system. The value of maximum efficiency attained by the three-phase system is higher than that of two-phase system.
- Also from the electromechanical characteristics, the speed – torque characteristics are linear which implies that the performance of the motors is hardly influenced by the winding inductance.
- The current – torque characteristics of the motors are linear which implies that the electromagnetic flux of the machine is hardly influenced by the armature reaction. This is due to the arrangement of strong rectangular shaped permanent magnets on the rotor discs which reduces the armature reaction.
- At rated torque $T_l = 10\ N{\cdot}m$, the current drawn by the three-phase motor is 9.55 A and that of 11.7 A in case of two-phase motor which results in copper losses and heating effects. Hence, the overall efficiency is reduced.
- The maximum speed attained at $T_l = 10\ N{\cdot}m$ by the three-phase motor is 140.85 rpm and that of 164.44 rpm in case of two-phase motor which implies that by increasing the number of phases in the winding connection, the maximum speed attained by the motor gets reduced. In three-phase motor, the maximum steady – state speed is attained in 0.03 seconds and whereas in two-phase system, it is attained in 0.07 seconds. Hence, the three-phase

system comes into stead – state in relatively shorter time than that of two-phase system.

- Based on the simulation results of the two motors, by varying the commutation angle of the transistors in the inverter circuit, the efficiency of the motors could be greatly varied. Both the motors, from the simulation of the models, attain maximum efficiency at switching angle $\beta = -10°$. The maximum efficiency for three-phase system is 88.36 % and for two-phase it is 87.8 %. So by advancing the commutation angle, the efficiencies could be greatly improved. Also, it prevents the electromagnetic torque T_{em} from going into negative values.

References

1. http://www.electricmotors.machinedesign.com/guiEdits/Content/bdeee3/bdeee3_3.aspx

2. Large Brushless Drive Systems: Is there one in your future? – http://powertecmotors.com/a0201el.pdf

3. Application of brushless DC drives for blow molding – http://powertecmotors.com/ablowe2.pdf

4. Jacek F. Gieras, Rong-Jie Wang, Maarten J. Kamper, *Axial flux permanent magnet brushless machines,* Kluwer Academic Publishers, 2005

5. http://services.eng.uts.edu.au/~joe/subjects/ems/ems_ch12_nt.pdf

6. Aydin, M., S. Huang, T.A. Lipo, "Axial Flux Permanent Magnet Disc Machines: A Review, Symposium on Power Electronics", Electrical Drives, Automation, and Motion (SPEEDAM) 2004, Capri, Italy, June 16-18, 2004.

7. E. Spooner, B. J. Chalmers, M. M. El-Missiry, Wu Wei, and A. C. Renfrew, "Motoring performance of the toroidal permanent magnet machine 'TORUS'", *IEE International Conference on Electrical Machines and Drives,* London, UK, September, 1991, pp. 36-40.

8. E. Spooner and B. J. Chalmers, "TORUS, a slotless, toroidal-stator, permanent magnet generator", *Proc. IEE, Part-B, Vol.139, No. 6, Nov. 1992, pp. 497-506*.

9. R. Krishnan, *Electric Motor Drives Modeling, Analysis and Control*, Prentice Hall, Inc., 2001.

10. R. Drzewoski and E. Mendrela, "Torus type brushless D.C. motor as a gearless drive for electric vehicles".

11. Bumby, J.R., Martin, R., Spooner, E., Brown, N.L. and Chalmers, B.J., "Electromagnetic design of axial flux permanent magnet machines", Proc. IEE Electr. Power Applications, Vol. 151, March 2004, pp 151-160.

12. Mendrela E.A., Beniak R., Wróbel R, "Influence of Stator Structure on Electromechanical Parameters of Torus-type Brushless DC Motor", IEEE

Transactions on Energy Conversion, (PE-386EC (3-2002)), Vol. 18, No. 2, June 2003.

13. W Wu, E Spooner, and BJ Chalmers, “Design of slotless TORUS generators with reduced voltage regulation”, *IEE Proc. B,* Vol. 142, No. 5, 1995, pp. 337-343.

14. M. M. Elmissiry, S. Chari “Dynamic Performance of a Permanent Magnet, Axial Flux, Toroidal Stator, Brushless D.C.Motor.”1992.

15. T. Salem, T.A. Haskew, "Simulation of the brushless DC machine," *ssst*, p. 18, 27th Southeastern Symposium on System Theory (SSST'95), 1995.

16. Ernest A. Mendrela and Mariusz Jagiela, “Analysis of torque developed in axial flux, single-phase brushless DC motor with salient-pole stator”, IEEE transactions on energy conversion, Vol. 19, No. 2, June 2004, pp 271-277.

Appendix A: Matlab Programs for Three Phase Motor

Program 1:

```
%Electromechanical characteristics of the motor (Dynamic State)
% TL - T_load
% pin - Input power
% Pem - Mechanical Power
% is - Source Current
% ia - Armature Current
% w - Speed
% eff - efficiency
% Tem - Electromagnetic Torque

% Switching angle Beta=+20

TL=[0 0.5 1 1.5 2 2.5 3 4 5 8 10 11];
pin4=[17.5 31 44.2 58 71 84.8 98 124 150 229 280.8 306.2];
pem4=[0 10.3 20.1 29.4 38.3 46.7 54.72 69.57 82.95 115.5 131.7 138.39];
is4=[0.74 1.3 1.85 2.4 2.96 3.52 4.06 5.17 6.25 9.53 11.7 12.76];
ia4=[2 2.25 2.57 3 3.4 3.85 4.25 5.15 6 8.81 10.65 11.54];
w4=[21.11 20.6 20.1 19.6 19.14 18.7 18.25 17.4 16.59 14.43 13.16 12.58];
eff4=[0 33.23 45.48 50.69 53.94 55.07 55.84 56.1 55.3 50.44 46.9 45.2];
Tem4=[0.08 0.58 1.08 1.58 2.08 2.57 3.06 4.07 5.07 8.05 10.05 11.05];

% Switching angle Beta=-20

TL = [0 0.5 1 1.5 2 2.5 3 4 5 8 10 11];
pin5 = [15 25.6 36.4 47 58 69 79.5 101.5 123.3 189 232.6 255];
pem5 = [0 12.9 25.2 36.9 48.05 58.66 68.7 87.5 104.5 146 166.9 175.6];
is5 = [0.61 1.07 1.51 1.95 2.41 2.88 3.33 4.23 5.14 7.87 9.7 10.62];
ia5 = [2.82 2.77 2.76 2.8 2.95 3.15 3.37 3.9 4.53 6.65 8.2 8.98];
w5 = [26.45 25.8 25.2 24.6 24.02 23.46 22.9 21.87 20.9 18.24 16.7 15.95];
eff5 = [0 50.39 69.23 78.51 82.84 85.01 86.42 86.21 84.75 77.25 71.75 68.86];
Tem5 = [0.08 0.58 1.08 1.58 2.08 2.57 3.06 4.07 5.07 8.05 10.05 11.05];

% Switching angle Beta=0

TL = [0 0.5 1 1.5 2 2.5 3 4 5 8 10 11];
pin1 = [11.05 21.6 31.7 41.35 50.6 59.4 75.88 90.9 128.25 147.5 155.7];
```

```
pem1 = [0 11.05 21.6 31.7 41.35 50.6 59.4 75.88 90.9 128.25 147.5 155.7];
is1 = [0.2 0.75 1.35 1.9 2.5 3.1 3.65 4.7 6 9.4 11.7 12.9];
ia1 = [1.18 1.2 1.3 1.54 1.85 2.2 2.56 3.35 4.15 6.6 8.25 9.05];
w1 = [22.6 22.1 21.6 21.1 20.7 20.3 19.8 18.97 18.2 16.03 14.75 14.2];
eff1 = [0 73.67 83.08 84.53 85.17 84.33 83.08 80.55 77.96 69.51 64.13 61.79];
Tem1 = [0.08 0.58 1.08 1.58 2.08 2.57 3.06 4.07 5.07 8.05 10.05 11.05];

% Switching angle Beta= +10

TL = [0 0.5 1 1.5 2 2.5 3 4 5 8 10 11];
pin2 = [7 19 31 43.2 55.1 67.1 79.4 103.5 127.6 199.5 247 270.6];
pem2 = [0 10.57 20.68 30.33 39.52 48.33 56.7 72.4 86.6 121.8 139.7 147.24];
is2 = [0.27 0.73 1.17 1.63 2.09 2.54 2.99 3.91 4.83 7.56 9.4 10.32];
ia2 = [1.1 1.28 1.55 1.9 2.3 2.7 3.1 3.95 4.8 7.4 9.11 9.97];
w2 = [21.65 21.16 20.7 20.22 19.78 19.33 18.9 18.08 17.31 15.21 14 13.39];
eff2 = [0 55.63 66.71 70.21 71.72 72.03 71.41 69.95 67.87 61.05 56.56 54.41];
Tem2 = [0.08 0.58 1.08 1.58 2.08 2.57 3.06 4.07 5.07 8.05 10.05 11.05];

% Switching angle Beta=-10

TL = [0 0.5 1 1.5 2 2.5 3 4 5 8 10 11];
pin3 = [6.4 17.1 28 39 50 61 71.9 94 116 181.5 225.4 247.3];
pem3 = [0 11.77 23.4 33.79 44.08 53.9 63.25 80.7 96.63 136.1 156.4 164.9];
is3 = [0.27 0.73 1.17 1.63 2.09 2.54 2.99 3.91 4.83 7.56 9.4 10.32];
ia3 = [1.95 1.87 1.9 2.02 2.2 2.44 2.73 3.35 4.1 6.38 7.95 8.74];
w3 = [24.1 23.58 23.4 22.52 22.04 21.55 21.1 20.19 19.32 17.01 15.6 14.9];
eff3 = [0 68.83 83.57 86.64 88.16 88.36 87.97 85.85 83.3 74.99 69.39 66.68];
Tem3 = [0.08 0.58 1.08 1.58 2.08 2.57 3.06 4.07 5.07 8.05 10.05 11.05];



figure(1)
plot(TL,eff2,'-r*',TL,eff3,'-b^',TL,eff1,'-ko',TL,eff4,'-go',TL,eff5,'-md'), grid
xlabel('TL[N.m]');
ylabel('%Efficiency');
legend('Beta=+10','Beta=-10','Beta=0','Beta=+20','Beta=-20',4)


figure(2)
plot(TL,is2,'-r*',TL,is3,'-b^',TL,is1,'-ko',TL,is4,'-go',TL,is5,'-md'), grid
xlabel('TL[N.m]');
ylabel('supply current');
legend('Beta=+10','Beta=-10','Beta=0','Beta=+20','Beta=-20',4)
```

```
figure(3)
plot(TL,pem2,'-r*',TL,pem3,'-b^',TL,pem1,'-ko',TL,pem4,'-go',TL,pem5,'-md'), grid
xlabel('TL[N.m]');
ylabel('mechanical power output');
legend('Beta=+10','Beta=-10','Beta=0','Beta=+20','Beta=-20',4)

%electromechanical characteristics of the motor for Beta = -10

figure(4)
plot(TL,eff3,'-r*',TL,is3*10,'-b^',TL,pem3,'-ko',TL,w3*5,'-go'), grid
title('Electromechanical characteristics of the motor for Beta = -10')
xlabel('TL[N.m]');
legend('%efficiency','source current/10','electromechanical power','speed/5',1,4)
```

Program 2:

```
% Emfs and phase voltage plot

load voltage_phase Va; load emfa Ea; load emfb Eb; load emfc Ec;
Va=Va',Ea=Ea';Eb=Eb';Ec=Ec';
t=Va(:,1); va=Va(:,2); e=Ea(:,2);e1=Eb(:,2);e2=Ec(:,2);

figure(1);
plot(t,va,t,e,t,e1,t,e2,'g'),xlabel('time (sec)'),ylabel('Va, ea , eb, ec (V)'),grid,gtext('Va'),
gtext('ea'),gtext('eb'),gtext('ec')
```

Program 3:

```
% Simulation results-steady state model

Is=0:0.1:12; Kms=1.21;
Us=24;Ra=0.25;
Ps=Us*Is;
Ts=Is*Kms;
omgas=(Us-Ra*Is)./(0.87*Kms+0.052*Is);
ns=omgas*30/pi;
Pms=(Ts-omgas*0.004).*omgas;
Tsh=Ts-omgas*0.004;
Effs=0.85*Pms./Ps*100;
```

```
% simulation results from dynamic model
Td=[0 0.5 1 1.5 2 2.5 3 4 5 8 10 11];
Effd=[0 73.67 83.08 84.53 85.17 84.33 83.08 80.55 77.96 69.51 64.13 61.79];
Pmd=[0 11.05 21.6 31.7 41.35 50.6 59.4 75.88 90.9 128.25 147.5 155.7];
Id=[1.18 1.2 1.3 1.54 1.85 2.2 2.56 3.35 4.15 6.6 8.25 9.05];
omgad=[22.6 22.1 21.6 21.1 20.7 20.3 19.8 18.97 18.2 16.03 14.75 14.2];
nd=omgad*30/pi;
Tem=Td+0.5;


figure(1)

plot(Tsh,10*Is,'r',Td,10*Id,'r*',Tsh,ns,'g',Tsh,Pms,'k',Td,nd,'go',Td,Pmd,'kx'),grid,
xlabel('Torque  [N.m]'),
gtext('speed  [r.p.m.]'),gtext('Output power  [W]'),gtext('current/10 [A]')
legend('from steady-state','from dynamic-state')

figure(2)

plot(Tsh,Effs,'r',Tsh,10*Is,'g',Ts,ns,'b',Tsh,Pms/1,'k'),grid,
xlabel('torque  [N.m]'),
gtext('efficiency  [%]'),gtext('Speed  [r.p.m.]'), gtext('Mechanical power
[W]'),gtext('Current*10 [A]')
```

Appendix B: Matlab Programs for Two Phase Motor

Program 1:

```
%Electromechanical characteristics of the two phase motor (Dynamic State)
% TL - T_load
% pin - Input power
% Pem - Mechanical Power
% is - Source Current
% ia - Armature Current
% w - Speed
% eff - efficiency
% Tem - Electromagnetic Torque

% Switching angle Beta=+20

TL = [0 0.5 1 1.5 2 2.5 3 4 5 8 10 11];
pin4 = [12.4 28.6 48 61 76 93 109 140 173 268 330 362];
pem4 = [0 13.01 25.28 36.85 47.8 58.1 67.9 85.75 101.7 139.6 158.4 165.9];
is4 = [0.53 1.19 1.85 2.53 3.2 3.88 4.5 5.9 7.2 11.2 13.8 15.1];
ia4 = [1.3 1.6 2.1 2.5 2.9 3.48 3.9 5 5.9 8.8 10.8 11.95];
w4 = [26.79 26.01 25.28 24.58 23.9 23.25 22.6 21.44 20.33 17.45 15.83 15.09];
eff4 = [0 45.49 52.67 60.41 62.89 62.47 62.29 61.25 58.79 52.09 48 45.83];
Tem4 = [0.1 0.6 1.1 1.6 2.1 2.6 3.1 4.1 5.1 8 10 11.1];

% Switching angle Beta=-20

TL = [0 0.5 1 1.5 2 2.5 3 4 5 8 10 11];
pin5 = [12 25 39 52 66 79 93 119.5 148 229.5 284.5 312.4];
pem5 = [0 15.48 30.1 43.85 57 69.3 81 102.5 121.6 167.5 193 199.6];
is5 = [0.45 1.1 1.6 2.15 2.75 3.3 3.83 5 6.15 9.58 11.86 13.2];
ia5 = [1.5 1.57 1.6 1.9 2.1 2.51 2.9 3.7 4.52 7.19 8.87 9.75];
w5 = [31.9 30.9 3.1 29.3 28.5 27.72 27 25.61 24.31 20.94 19.02 18.15];
eff5 = [0 61.92 77.18 84.33 86.36 87.72 87.1 85.77 82.16 72.98 67.84 63.89];
Tem5 = [0.1 0.6 1.1 1.6 2.1 2.6 3.1 4.1 5.1 8 10 11.1];

% Switching angle Beta=0

TL = [0 0.5 1 1.5 2 2.5 3 4 5 8 10 11];
pin1 = [5 18 32.5 46 60 74 87 116 143.5 226 281 310];
pem1 = [0 13.5 26.4 38.5 50 61 71.5 90.8 108 150.7 172.5 181];
is1 = [0.2 0.75 1.35 1.9 2.5 3.1 3.65 4.7 6 9.4 11.7 12.9];
```

```
ia1 = [0.5 0.65 1 1.45 1.9 2.3 2.7 3.6 4.5 7.3 9.1 9.8];
w1 = [27.7 27 26.34 25.6 25.1 24.43 23.8 22.7 21.64 18.8 17.22 16.5];
eff1 = [0 75 81.23 83.7 83.3 82.43 82.18 78.28 75.26 66.68 61.39 58.39];
Tem1 = [0.1 0.6 1.1 1.6 2.1 2.6 3.1 4.1 5.1 8 10 11.1];

% Switching angle Beta=+10

TL = [0 0.5 1 1.5 2 2.5 3 4 5 8 10 11];
pin2 = [7 21.5 35.8 51 65 80 95 123 153 241 300 327];
pem2 = [0 13.1 25.5 37.3 48.5 59.1 69.1 87.7 104.5 145 165 174];
is2 = [0.29 0.9 1.5 2.1 2.7 3.3 3.9 5.2 6.4 10 12.5 13.6];
ia2 = [0.62 0.95 1.3 1.8 2.25 2.6 3.2 4.2 5.1 7.9 9.7 10.7];
w2 = [26.95 26.2 25.6 24.9 24.25 23.6 23.05 21.9 20.9 18.1 16.5 15.8];
eff2 = [0 60.93 71.23 73.14 74.62 73.88 72.74 71.3 68.3 60.17 55 53.21];
Tem2 = [0.1 0.6 1.1 1.6 2.1 2.6 3.1 4.1 5.1 8 10 11.1];

% Switching angle Beta=-10

TL = [0 0.5 1 1.5 2 2.5 3 4 5 8 10 11];
pin3 = [6 20 33.33 46.9 60 74 87.5 115 142 223 277 305];
pem3 = [0 14.26 27.8 40.6 52.7 64.3 75.3 95.5 113.7 158 180.4 190];
is3 = [0.3 0.85 1.388 1.95 2.5 3.1 3.65 4.8 5.9 9.3 11.5 12.7];
ia3 = [0.95 0.98 1.185 1.5 1.8 2.2 2.7 3.5 4.4 7 8.8 9.6];
w3 = [29.3 28.5 27.8 27.08 26.4 25.5 25.1 23.9 22.8 19.75 18.05 17.25];
eff3 = [0 71.3 83.41 86.57 87.8 86.89 86.06 83.04 80.07 70.85 65.13 62.3];
Tem3 = [0.1 0.6 1.1 1.6 2.1 2.6 3.1 4.1 5.1 8 10 11.1];



figure(1)
plot(TL,n2,'-r*',TL,n3,'-b^',TL,n1,'-ko',TL,n4,'-go',TL,n5,'-md'), grid
xlabel('TL[N.m]');
ylabel('%efficiency');
legend('Beta=+10','Beta=-10','Beta=0','Beta=+20','Beta=-20',4)

figure(2)
plot(TL,is2,'-r*',TL,is3,'-b^',TL,is1,'-ko',TL,is4,'-go',TL,is5,'-md'), grid
xlabel('TL[N.m]');
ylabel('supply current');
legend('Beta=+10','Beta=-10','Beta=0','Beta=+20','Beta=-20',4)

figure(3)
plot(TL,pem2,'-r*',TL,pem3,'-b^',TL,pem1,'-ko',TL,pem4,'-go',TL,pem5,'-md'), grid
xlabel('TL[N.m]');
```

```
ylabel('mechanical power output');
legend('Beta=+10','Beta=-10','Beta=0','Beta=+20','Beta=-20',4)

%electromechanical characteristics of the motor for Beta = -10
figure(4)
plot(TL,n3,'-r*',TL,is3*10,'-b^',TL,pem3,'-ko',TL,w3*5,'-go'), grid
title('Electromechanical characteristics of the motor for Beta = -10')
xlabel('TL[N.m]');
legend('%efficiency','source current*10','electromechanical power','speed*5',1,4)
```

Program 2:

```
load voltage_phase Va; load emf Ea; load emfb Eb;
Va=Va',Ea=Ea';Eb=Eb';
t=Va(:,1); va=Va(:,2); e=Ea(:,2);e1=Eb(:,2);

figure(1);

plot(t,va,t,e,t,e1,'g'),xlabel('time (sec)'),ylabel('Va, Ea , Eb(V)'),grid,gtext('Va'),
gtext('Ea'),gtext('Eb')
```

Program 3:

```
%simulation results-steady state model

%Is=1:1:12; Kms=1.143;
%Us=24;Rs= 0.0005;
%Ps=Us*Is;
%Ts=Is.*Kms;
%omgas=(Us-Rs*Is)./(Kms);
%ns=omgas*30/pi;
%Pms=(Ts-omgas*.004).*omgas; %D=0.004
%Effs=Pms./Ps*100;

Is=0:0.1:12; Kms=1.12;
Us=24;Ra=0.25;
Ps=Us*Is;
Ts=Is*Kms;
omgas=(Us-Ra*Is)./(0.77*Kms+0.045*Is);
ns=omgas*30/pi;
Pms=(Ts-omgas*0.004).*omgas;
```

```
Tsh=Ts-omgas*0.004;
Effs=0.75*Pms./Ps*100;

% simulation results from dynamic model

Td = [0 0.5 1 1.5 2 2.5 3 4 5 8 10 11];
effd = [0 75 81.23 83.7 83.3 82.43 82.18 78.28 75.26 66.68 61.39 58.39];
Pmd = [0 13.5 26.4 38.5 50 61 71.5 90.8 108 150.7 172.5 181];
Id = [0.5 0.65 1 1.45 1.9 2.3 2.7 3.6 4.5 7.3 9.1 9.8];
omgad = [27.7 27 26.34 25.6 25.1 24.43 23.8 22.7 21.64 18.8 17.22 16.5];
nd = omgad*30/pi;

xlabel('Torque  [N.m]'),
gtext('speed  [r.p.m.]'),gtext('Output power  [W]'),gtext('current/10 [A]')
legend ('from steady-state','from dynamic-state')
```

Appendix C: SIMULINK Block Diagrams for Three Phase

Subsystem For Logic Block:

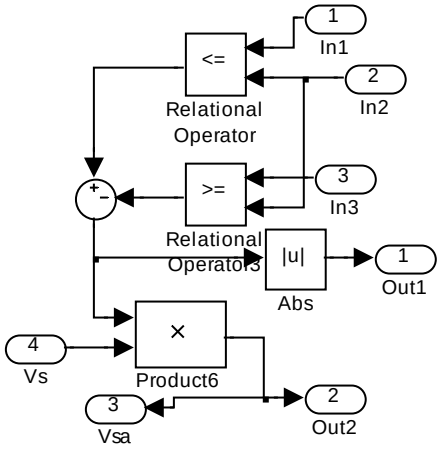

Subsystem For Electrical System (Phase A):

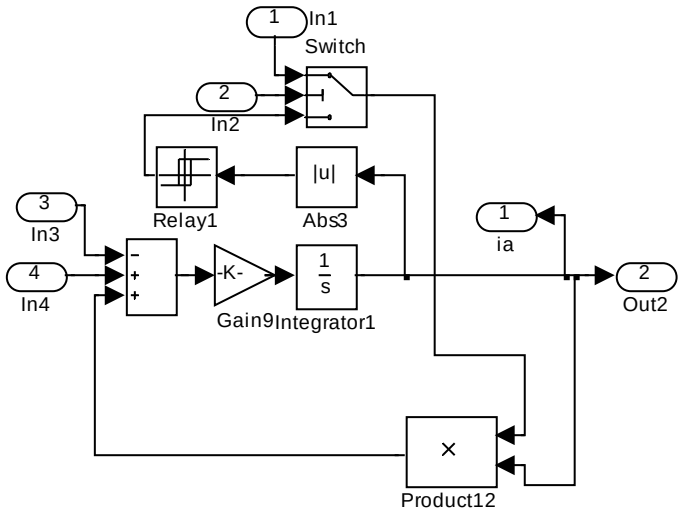

Appendix D: SIMULINK Block Diagrams for Two Phase

Subsystem For Logic Block:

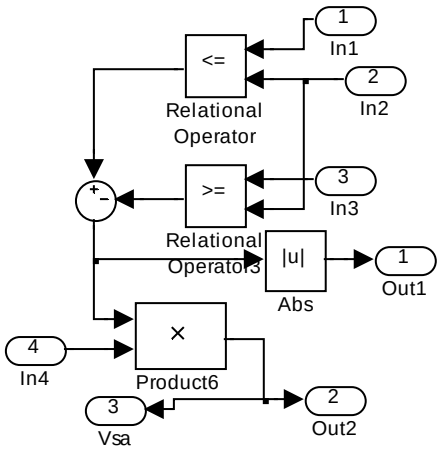

Subsystem for electrical system (phase A):

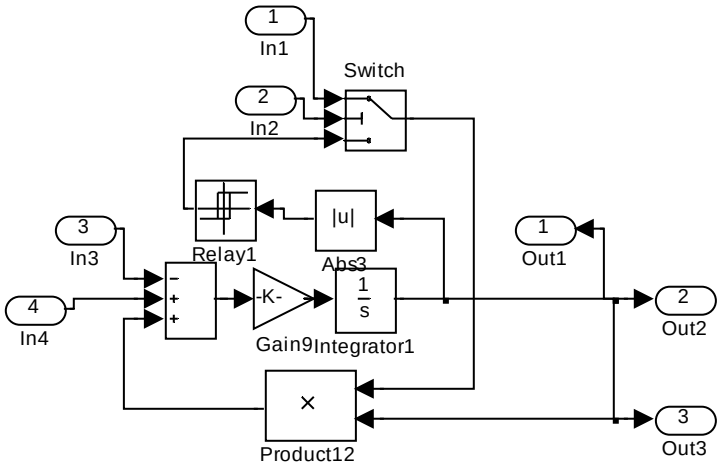

Vita

Dinakar Choppa was born on January 1st, 1982, in Visakhapatnam City, Andhra Pradesh, India. He finished his undergraduate studies at Andhra University in April 2003. In August 2004 he came to Louisiana State University to pursue graduate studies in electrical engineering. He is currently a candidate for the degree of Master of Science in Electrical Engineering, which will be awarded in August 2006.